

# A Signaling Polypeptide Derived from an Innate Immune Adaptor Molecule Can Be Harnessed as a New Class of Vaccine Adjuvant<sup>1</sup>

Kouji Kobiyama,<sup>3\*</sup> Fumihiko Takeshita,<sup>2,3\*</sup> Ken J. Ishii,<sup>†§</sup> Shohei Koyama,<sup>‡§</sup> Taiki Aoshi,<sup>†</sup> Shizuo Akira,<sup>‡§</sup> Asako Sakaue-Sawano,<sup>¶</sup> Atsushi Miyawaki,<sup>¶</sup> Yuko Yamanaka,<sup>||</sup> Hisashi Hirano,<sup>||</sup> Koichi Suzuki,<sup>#</sup> and Kenji Okuda\*

Modulation of intracellular signaling using cell-permeable polypeptides is a promising technology for future clinical applications. To develop a novel approach to activate innate immune signaling by synthetic polypeptides, we characterized several different polypeptides derived from the caspase recruitment domain (CARD) of IFN- $\beta$  promoter stimulator 1, each of which localizes to a different subcellular compartment. Of particular interest was, N'-CARD, which consisted of the nuclear localization signal of histone H2B and the IFN- $\beta$  promoter stimulator 1CARD and which localized to the nucleus. This polypeptide led to a strong production of type I IFNs and molecular and genetic analyses showed that nuclear DNA helicase II is critically involved in this response. N'-CARD polypeptide fused to a protein transduction domain (N'-CARD-PTD) readily transmigrated from the outside to the inside of the cell and triggered innate immune signaling. Administration of N'-CARD-PTD polypeptide elicited production of type I IFNs, maturation of bone marrow-derived dendritic cells, and promotion of vaccine immunogenicity by enhancing Ag-specific Th1-type immune responses, thereby protecting mice from lethal influenza infection and from outgrowth of transplanted tumors in vivo. Thus, our results indicate that the N'-CARD-PTD polypeptide belongs to a new class of vaccine adjuvant that directly triggers intracellular signal transduction by a distinct mechanism from those engaged by conventional vaccine adjuvants, such as TLR ligands. *The Journal of Immunology*, 2009, 182: 1593–1601.

Accumulating evidence from basic research and from clinical studies clearly indicates that type I IFNs are key to the elimination of viral infection (1, 2), suppression of tumor progression (3, 4), and to vaccine immunogenicity (5). Type I IFNs, such as IFN- $\alpha$  and - $\beta$ , are produced from a wide variety of cell types upon viral infection or in response to foreign nucleic acids, such as DNA and RNA (6–8). Recent research has dissected and elucidated the molecular basis of the ability of the immune system to sense a variety of nucleic acids as pathogen-associated molecular patterns (9) or to sense the presence of aberrant self-DNA under dangerous situations (10, 11). RIG-I-like helicases

(RLHs)<sup>4</sup> mediate innate immune signaling in human cells induced by immunostimulatory RNAs, such as 5'-triphosphate RNA or dsRNA, or right-handed B-form DNA (B-DNA) (12–14). RLHs trigger cellular signaling through adaptor molecules, such as IFN- $\beta$  promoter stimulator 1 (IPS-1, also known as MAVS/VISA/Cardif), TNFR-associated factor (TRAF) 3, and TRAF family member-associated NF- $\kappa$ B activator (TANK), thereby coordinating the activation of I $\kappa$ B kinase (IKK) family members, such as NF- $\kappa$ B essential modulator, IKK- $\alpha$ , IKK- $\beta$ , TANK-binding kinase 1 (TBK1), and inducible IKK (IKKi). Once activated by such cytoplasmic kinases, NF- $\kappa$ B, IFN regulatory factor 3 (IRF3), and IRF7 translocate into the nucleus and act as master regulators of type I IFN-related gene promoters (15).

These signaling molecules contain distinct domains, and thereby associate with specific target molecules and modulate downstream signal transmission. IPS-1 plays a central role in this signaling pathway and its caspase recruitment domain (CARD) forms the death domain fold, which is structurally similar to domains of Fas-associated via death domain and caspase family members (16). The CARD of IPS-1 is essential for signal transmission through homotypic interactions with the CARDs of upstream RLHs (9). Mitochondrial sorting of IPS-1 is also crucial for its canonical

\*Department of Molecular Biodefense Research, Yokohama City University Graduate School of Medicine, Yokohama, Japan; <sup>†</sup>Department of Molecular Protozoology and <sup>‡</sup>Host Defense, Research Institute for Microbial Diseases, Osaka University, Suita, Japan; <sup>§</sup>World Premier International Immunology Frontier Research Center, Osaka University, Suita, Japan; <sup>¶</sup>Laboratory for Cell Function Dynamics, Advanced Technology Development Group, Brain Science Institute, RIKEN, Wako, Japan; <sup>||</sup>Kihara Institute for Biological Research, Yokohama City University Graduate School of Integrated Science, Totsuka, Japan; and <sup>#</sup>Department of Bioregulation, National Institute of Infectious Diseases, Higashimurayama-shi, Japan

Received for publication July 24, 2008. Accepted for publication November 19, 2008.

The costs of publication of this article were defrayed in part by the payment of page charges. This article must therefore be hereby marked *advertisement* in accordance with 18 U.S.C. Section 1734 solely to indicate this fact.

<sup>1</sup> This work was supported, in part, by the Strategic Research Project of Yokohama City University (K18022 to F.T.), the Advancement of Medical Sciences from Yokohama Medical Foundation (to F.T. and K.K.), the National Institute of Biomedical Innovation (to K.O.), the Yasuda Medical Foundation (to F.T.), the Uehara Memorial Foundation (to F.T.), and a Grant-in-aid for Scientific Research (20590477 to F.T.) from the Ministry of Education, Culture, Sports, Science, and Technology of Japan.

<sup>2</sup> Address correspondence and reprint requests to Dr. Fumihiko Takeshita, Department of Molecular Biodefense Research, Yokohama City University Graduate School of Medicine, 3-9 Fukuura, Kanazawaku, Yokohama, Japan. E-mail address: takesita@yokohama-cu.ac.jp

<sup>3</sup> K.K. and F.T. contributed equally to this work.

<sup>4</sup> Abbreviations used in this paper: RLH, RIG-I-like helicase; B-DNA, B-form DNA; IPS-1, IFN- $\beta$  promoter stimulator 1; TRAF, TNFR-associated factor; TANK, TRAF family member-associated NF- $\kappa$ B activator; TBK1, TANK binding kinase 1; IKK, I $\kappa$ B kinase; IKKi, inducible IKK; IRF3, IFN regulatory factor 3; CARD, caspase recruitment domain; N'-CARD, fusion of the NH<sub>2</sub>-terminal nuclear localization signal of histone H2B to the IPS-1 CARD; PTD, protein transduction domain; TMD, transmembrane domain; NLS, nuclear localization signal; NDH, nuclear DNA helicase II; ODN, oligodeoxynucleotide; flu vax, influenza split-product vaccine; DC, dendritic cell; FL, full length; BM-DC, bone marrow-derived dendritic cell.

Copyright © 2009 by The American Association of Immunologists, Inc. 0022-1767/09/\$2.00

signaling because human hepatitis C virus NS3/4A protease inactivates IPS-1 by cleaving a region adjacent to the transmembrane domain (TMD), which is required for IPS-1 localization to the mitochondrial outer membrane (17).

To develop a novel approach to modulate innate immune signaling by synthetic polypeptides, we generated several different IPS-1 CARD-fusion polypeptides, each of which localizes to a different subcellular compartment. Of interest, the nuclear localization of a fusion polypeptide between the nuclear localization signal (NLS) of histone H2B and the IPS-1 CARD (hereafter referred to as N'-CARD) activated a distinct signaling pathway initiated from the nucleus and led to a strong production of type I IFN. Molecular and genetic analyses showed that nuclear DNA helicase II (NDH) is critically involved in this signaling pathway. Fusion of N'-CARD to the protein transduction domain (PTD), originally derived from the HIV Tat protein (18), facilitated transduction of N'-CARD from outside to inside the cell without loss of its original intracellular function. Finally, we demonstrate that the N'-CARD-PTD polypeptide acts as a novel vaccine adjuvant by directly triggering innate intracellular immune signaling to augment vaccine immunogenicity. Such a mechanism is distinct from TLR-mediated signaling, which is engaged in innate immune activation by conventional vaccine adjuvants, such as monophosphoryl-lipid A (an LPS derivative) and CpG oligodeoxynucleotide (ODN).

## Materials and Methods

### Cells and reagents

HEK293, HeLa, RAW264.7, and TC-1 cells were purchased from American Type Culture Collection and maintained in DMEM supplemented with 10% FCS and 50  $\mu\text{g}/\text{ml}$  penicillin/streptomycin. Sf9 cells were maintained in Sf900 II SFM (Invitrogen). LPS was purchased from Sigma-Aldrich. CpG ODN, 5'-ATC GAC TCT CGA GCG TTC TC-3', was synthesized by Gene Design. Mouse GM-CSF and Flt3L were purchased from PeproTech. Influenza split-product vaccine (flu vax) was prepared at The Research Foundation for Microbial Diseases of Osaka University (Kanon-ji city, Kagawa, Japan) from the purified influenza virus A/New Caledonia/20/99 strain (H1N1) by sequential treatment with ether and formalin, according to the method of Davenport et al. (19, 20).

### Expression plasmids

The IPS-1 expression plasmid was described previously (21). The IPS-1 CARD, aa 1–100 of the IPS-1 ORF, was PCR-amplified. Fusion cDNAs were generated by ligating aa 1–100 and 514–540 of IPS-1 ORF (CARD-TMD), aa 1–37 of histone H2B ORF and aa 1–100 of IPS-1 ORF (N'-CARD), N'-CARD and aa 514–540 of hIPS-1 ORF (N'-CARD-TMD), and were amplified by PCR. These fragments were introduced in-frame into pFLAG CMV5b (Sigma-Aldrich) or pGEX6P-2 (GE Healthcare). GST-N'-CARD was further fused to the PTD (Tyr-Ala-Arg-Ala-Ala-Ala-Arg-Gln-Ala-Arg-Ala) and introduced into pFastBac HT-B (Invitrogen). TBK1, IKKi, NDH, and chloride channel 1A (CC1A) cDNAs were amplified by PCR using a human spleen cDNA library (Takara). These fragments were introduced in-frame into pFLAG-CMV4 (Sigma-Aldrich), pCIneo-HA, pCAGGS-Flag-m1SECFP, pCAG-His Venus, or pcDNA3-RFP. The N'-CARD T54A expression plasmid was generated by site-directed mutagenesis, as described previously (22). The sequences of the PCR products were confirmed using an ABI PRISM Genetic Analyzer (PE Applied Biosystems).

### Luciferase assay

The luciferase assay was conducted as described previously (23).

### Confocal microscopy

HeLa cells were transfected with CARD-YFP, CARD-TMD-YFP, N'-CARD-YFP, N'-CARD-TMD-YFP, IPS-1-YFP, YFP-IKKi, YFP-TBK1, and/or mRFP-NDH and incubated for 48 h. In some cases, the cells were treated with Hoechst 33258 (Invitrogen) and/or MitoTracker reagent (Invitrogen) at 37°C for 15 min. Alternatively, HeLa cells were treated with CARD or N'-CARD-PTD for 30 min. Cells were treated with Hoechst 33258 for 15 min before fixation and incubation with mouse anti-FLAG

M2-Cy3. After washing with PBS containing 1% BSA, the cells were examined under an FV 500 confocal microscope (Olympus).

### Immunoprecipitation and immunoblotting

Immunoprecipitation and immunoblotting was performed as described previously (24) using anti-FLAG M2 (Sigma-Aldrich), anti-FLAG M2-HRP (Sigma-Aldrich), anti-HA (Covance), anti-HA-HRP (Roche Diagnostics), anti-ubiquitin-HRP (Santa Cruz Biotechnology), anti-NDH (provided by J. D. Parvin, Brigham and Women's Hospital, Boston, MA), anti-p-JNK, anti-p-p38, anti-p-ERK, and anti- $\beta$ -actin (Cell Signaling Technology).

### RNA interference

An siRNA targeting NDH mRNA (stealth RNAi) was chemically synthesized by Invitrogen (Carlsbad, CA): sense, 5'-AUU GCU UGC AAA UCA UGA UCC UGU U-3'; antisense, 5'-AAC AGG AUC AUG AUU UGC AAG CAA U-3'. HEK293 cells ( $6 \times 10^5$ ) were transfected with 120 pmol of control or NDH siRNA using Lipofectamine RNAi MAX reagent (Invitrogen) according to the manufacturer's protocol.

### Purification of recombinant polypeptides

DH10Bac competent cells (Invitrogen) were transformed with pFastBac HT-B-GST or with GST-N'-CARD-PTD to generate recombinant Bacmids. Sf9 cells were transfected with Bacmid-encoding GST or GST-N'-CARD-PTD to generate recombinant seed baculoviruses. Seventy-two hours after infection, the Sf9 cells were washed once with PBS and suspended in sonication buffer (50 mM Tris-HCl (pH 8.0), 50 mM NaCl, 1 mM EDTA, 1 mM DTT) containing 10% Triton X-100. After sonication, cell lysates were centrifuged at 15,000 rpm, at 4°C for 30 min. The supernatants were collected and dialyzed with sonication buffer. Recombinant polypeptides were purified using GSTrap (GE Healthcare) according to the manufacturer's protocol. In brief, after the column was equilibrated with 2 ml sonication buffer, the cell lysate was applied and the column then washed three times with 10 ml PBST (PBS containing 0.5% Triton X-100) and with PBS once. Recombinant polypeptide (GST or GST-N'-CARD-PTD) was eluted with sonication buffer containing 10 mM reduced glutathione and then dialyzed with PBS. Recombinant proteins (1  $\mu\text{g}$ ) used in all the experiments contained <20 fg endotoxins (*Limulus* J Single Test, Wako).

### ELISA and RT-PCR

Bone marrow-derived dendritic cells (DCs) were generated by 5 days of culture with GM-CSF (20 ng/ml) (GM-DCs) or Flt3L (100 ng/ml) (FL-DCs). GM-DCs or FL-DCs were treated with or without 1, 3, or 10  $\mu\text{g}/\text{ml}$  N'-CARD-PTD or 1  $\mu\text{M}$  of CpG ODN for 24 h and the supernatants were subjected to ELISA for mouse IFN- $\alpha$ , IFN- $\beta$  (PBL Biomedical Laboratories), or IL-12 p40 (Invitrogen). RAW264.7 cells were treated with 1  $\mu\text{g}/\text{ml}$  LPS or 10  $\mu\text{g}/\text{ml}$  N'-CARD-PTD for 3, 6, 12, 18, 24, and 48 h. The levels of mRNA for TNF- $\alpha$ , IL-6, IFN- $\alpha$ , IFN- $\beta$ , IP-10, and  $\beta$ -actin were examined by RT-PCR as described previously (5, 22).

### Immunization

Eight-week-old female BALB/c mice were administered s.c. with N'-CARD-PTD (5  $\mu\text{g}$ ), CpG ODN (5  $\mu\text{g}$ ), or flu vax (0.7  $\mu\text{g}$ ) alone, flu vax (0.7  $\mu\text{g}$ ) plus N'-CARD-PTD (5  $\mu\text{g}$ ), or flu vax (0.7  $\mu\text{g}$ ) plus CpG ODN (5  $\mu\text{g}$ ) at 0 and 10 days. Blood was drawn at 20 days and serum Ab titer was measured by ELISA as described previously (25). Alternatively, 8-wk-old female C57BL/6 mice were immunized with E7 peptide (E7, Arg-Ala-His-Tyr-Asn-Ile-Val-Thr-Phe, 3  $\mu\text{g}$ ), E7 plus N'-CARD-PTD (5  $\mu\text{g}$ ), or E7 plus CpG ODN (5  $\mu\text{g}$ ) at 0 and 2 wk. Splenocytes were harvested 2 wk after final immunization. The cells were incubated with 1  $\mu\text{g}/\text{ml}$  E7 or NP peptide (Ala-Ser-Asn-Glu-Asn-Met-Glu-Thr-Met) for 18 h at 37°C. Total RNA was isolated and real-time PCR was performed as described previously (22).

### Influenza challenge

Ten days after final immunization, mice were challenged intranasally with  $2 \times 10^4$  pfu (8 LD<sub>50</sub>) of influenza virus A/PR/8/34 (25). The body weights and mortality of the challenged mice were monitored for the next 14 days.

### Tumor transplantation

Eight week-old C57BL/6 mice were administered subcutaneously with TC-1 ( $1 \times 10^5$  cells/mouse), a mouse lung carcinoma expressing E7 Ag (25). Mice were immunized with control NP peptide (3  $\mu\text{g}$ ), E7 (3  $\mu\text{g}$ ), N'-CARD-PTD (5  $\mu\text{g}$ ), or E7 (3  $\mu\text{g}$ ) plus N'-CARD-PTD (5  $\mu\text{g}$ ) at 3, 4, 5, 6, and 7 day after TC-1 inoculation. The sizes of local tumor mass were monitored for the next 20 days.

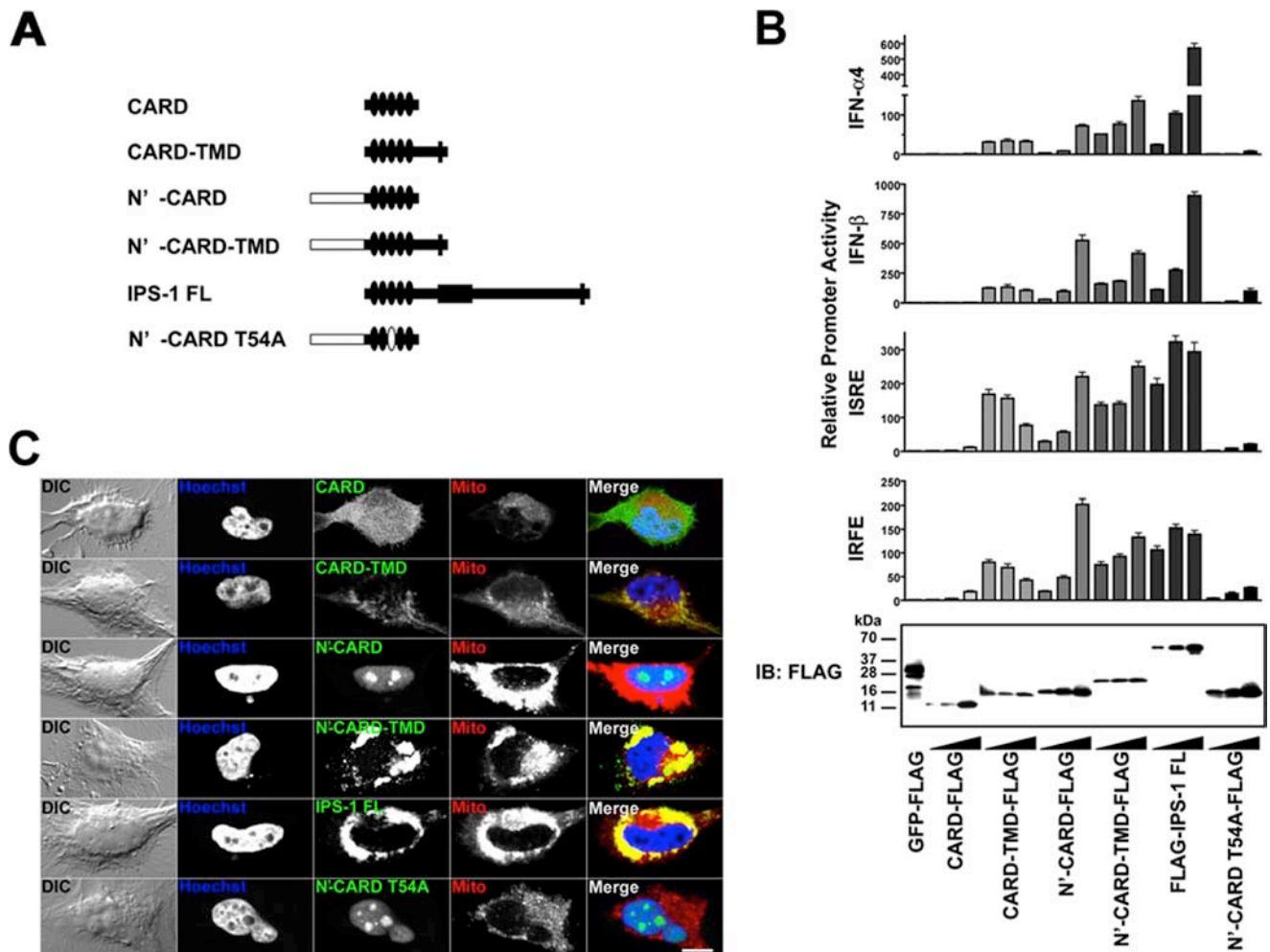


**FIGURE 1.** Synthetic IPS-1 CARD fusion molecules induce activation of type I IFN-related promoters. *A*, Schematic diagram of synthetic fusion molecules consisting of domains derived from IPS-1 and histone H2B. *B*, HEK293 cells were transfected with the expression plasmids, GFP-FLAG, CARD-FLAG, CARD-TMD-FLAG, N'-CARD-FLAG, N'-CARD-TMD-FLAG, FLAG-IPS-1 FL, and N'-CARD T54A-FLAG in the presence of TK-RL plus a reporter plasmid expressing firefly luciferase under the control of either the IFN- $\alpha$ 4 promoter (*top panel*), the IFN- $\beta$  promoter (*second panel from the top*), the ISRE-dependent promoter (*third panel from the top*), or the IRFE-dependent promoter (*fourth panel from the top*). Data represent means  $\pm$  SD of the relative luciferase activity of six samples. Cell lysates were also subjected to immunoblot analysis to examine levels of target polypeptide expression (*bottom panel*). *C*, HeLa cells were transfected with the expression plasmids, YFP-CARD, YFP-CARD-TMD, YFP-N'-CARD, YFP-N'-CARD-TMD, YFP-IPS-1 FL, and YFP-N'-CARD T54A. Genomic DNA or mitochondria were stained with Hoechst 33258 or Mitotracker reagent, respectively, and then analyzed under a confocal microscope. The data represent one of three independent experiments with similar results. Scale bar, 10  $\mu$ m.

#### Statistical analysis

The Student's *t* test or the Mantel-Cox log rank test was used for statistical analysis.

## Results

### *The nuclear redistribution of IPS-1 CARD elicits type I IFN promoter activation*

To elucidate the mechanisms underlying IPS-1 CARD-mediated signaling, plasmids encoding either the IPS-1 CARD alone or the IPS CARD fused to the IPS-1 TMD or to the NLS of histone H2B were generated and their abilities to induce type I IFN-related promoter activation were characterized (Fig. 1*A*). Although the CARD alone had minimal activity in eliciting such promoter activation, fusion of the TMD to the CARD (CARD-TMD) resulted in a significant activation, suggesting that the TMD facilitates CARD-mediated signaling, consistent with previous data (Fig. 1*B*; Ref. 26). Of interest, fusion of the NH<sub>2</sub>-terminal NLS of histone H2B to the IPS-1 CARD (N'-CARD) conferred strong promoter activation, suggesting that nuclear localization of N'-CARD trig-

gers signal activation. Indeed, N'-CARD induced phosphorylation of IRF3 at a comparable level to full length IPS-1 (FL) (Supplemental Fig. 1).<sup>5</sup> The mutant polypeptide N'-CARD T54A, in which the third  $\alpha$ -helical structure of the CARD was disrupted (22), induced significantly lower levels of promoter activation, suggesting that the conformation of the IPS-1 CARD is also critical for its activity. Although N'-CARD fused to the IPS-1 TMD (N'-CARD-TMD) induced significant levels of promoter activation, the levels were comparable to those induced by N'-CARD or CARD-TMD, suggesting that the effects of CARD distribution mediated by the NLS and the IPS-1 TMD are redundant.

### *N'-CARD localizes to the nucleus and signals through NDH*

To elucidate the signaling mechanisms triggered by N'-CARD and CARD-TMD, we examined the subcellular localizations of these fusion molecules. Confocal microscopy analysis showed that CARD-TMD fused to YFP (YFP-CARD-TMD) was present in

<sup>5</sup> The online version of this article contains supplemental information.

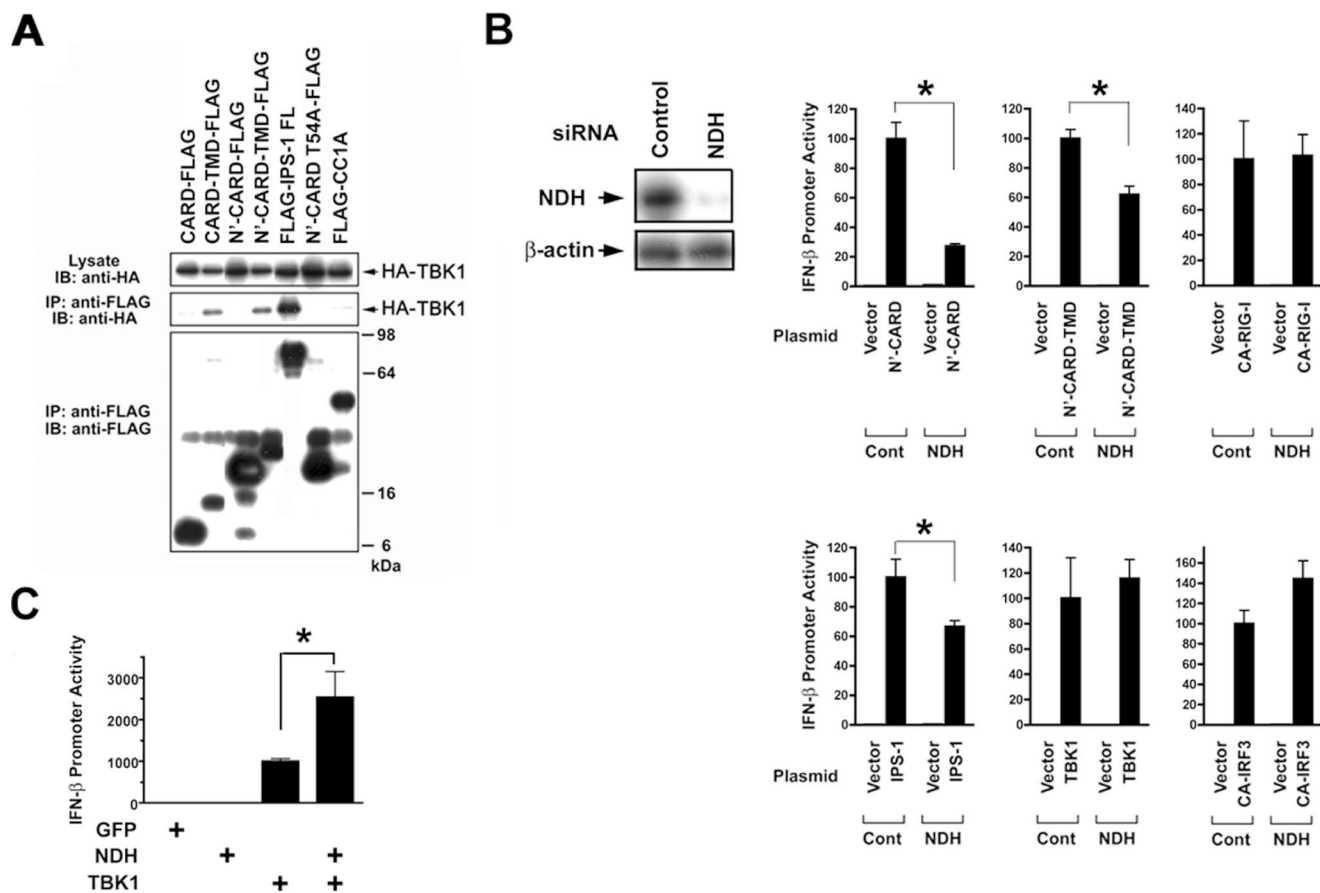


**FIGURE 2.** Role of NDH in N'-CARD-mediated signaling. *A*, Cell lysates from HEK293 cells transfected with the expression plasmids for HA-TBK1 plus CARD-FLAG, CARD-TMD-FLAG, N'-CARD-FLAG, N'-CARD-TMD-FLAG, FLAG-IPS-1 FL, N'-CARD T54A-FLAG, or FLAG-CC1A were prepared and immunoprecipitated with anti-FLAG Ab. The immune complexes were analyzed by immunoblotting using anti-HA or anti-FLAG Ab. *B*, After HEK293 cells were transfected with control or NDH siRNA, the levels of NDH protein were examined by immunoblotting. The cells were further transfected with the expression plasmid for N'-CARD, N'-CARD-TMD, CA-RIG-I, IPS-1, TBK1, and CA-IRF3 in the presence of TK-RL plus a reporter plasmid expressing firefly luciferase under the control of the IFN- $\beta$  promoter. *C*, HEK293 cells were transfected with the expression plasmid(s) for GFP, NDH, and/or TBK1 in the presence of TK-RL plus a reporter plasmid expressing firefly luciferase under the control of the IFN- $\beta$  promoter. *B* and *C*, Forty eight hours after transfection, luciferase assay was performed. Data represent means  $\pm$  SD of the relative luciferase activity of eight samples. \*,  $p < 0.05$ .

mitochondria, with a localization pattern similar to that of IPS-1 FL (YFP-IPS-1 FL), while N'-CARD fused to YFP (YFP-N'-CARD) was mostly present in the nuclear interchromosomal space (Fig. 1C). Because CARD alone (YFP-CARD) was present diffusely within the cell and both YFP-N'-CARD and YFP-N'-CARD T54A localized to the nucleus, it was suggested that the NLS directed the nuclear distribution of the IPS-1 CARD (Fig. 1C). These results implied that N'-CARD triggers cellular signaling pathways that originate in the nucleus and that are distinct from those triggered by CARD-TMD or IPS-1 FL, which originate from mitochondria.

TBK1, and its closely related IKK family member IKK $\alpha$ , are kinases acting downstream of IPS-1 and are required for a type I IFN production (21, 26, 27). We next examined the molecular interactions between each CARD-fusion molecule and TBK1 by immunoprecipitation analysis. As a control, TBK1 was coprecipitated with IPS-1 FL (Fig. 2A). A significant amount of TBK1 was also detected after precipitation with CARD-TMD or N'-CARD-TMD, but not after precipitation with CARD, N'-CARD, or N'-CARD T54A, suggesting that the TMD supports the association of the CARD with TBK1 (Fig. 2A).

To examine the signaling mechanisms triggered by N'-CARD, we tried to identify cellular molecules that associate with N'-CARD using a tandem-affinity purification system and TOF-MS

analysis (data not shown). Among the N'-CARD interacting molecules identified, we were particularly interested in nuclear DNA helicase II (NDH, also known as RNA helicase A), a 1270 amino acid protein containing two copies of a dsRNA binding domain, a DEIH (Asp-Glu-Ile-His) helicase core, and an RGG (Arg-Gly-Gly) box nucleic acid-binding domain.

To examine the functional role of NDH in the signaling pathway leading to type I IFN production, NDH mRNA was ablated by RNA interference. Endogenous NDH protein was specifically decreased by NDH siRNA but not by control siRNA treatment (Fig. 2B). Knockdown of NDH resulted in a suppression of N'-CARD-induced IFN- $\beta$  promoter activation by 73%. The level of promoter activation induced by IPS-1 or N'-CARD-TMD was also partially suppressed in NDH-knockdown cells by 33 and 38%, respectively. The levels were comparable when a constitutively active form of RIG-I (RIG-I 2CARDs), TBK1, or a constitutively active form of IRF3 (IRF3CA) was examined (Fig. 2B). Although over-expression of NDH had no effect, and over-expression of TBK-1 had a minimal effect on IFN- $\beta$  promoter activation, over-expression of NDH plus TBK1 synergistically activated the IFN- $\beta$  promoter, suggesting that NDH had the ability to up-regulate TBK1 activity (Fig. 2C). These results, taken together, suggest that NDH is involved in the events downstream of N'-CARD, and partially in

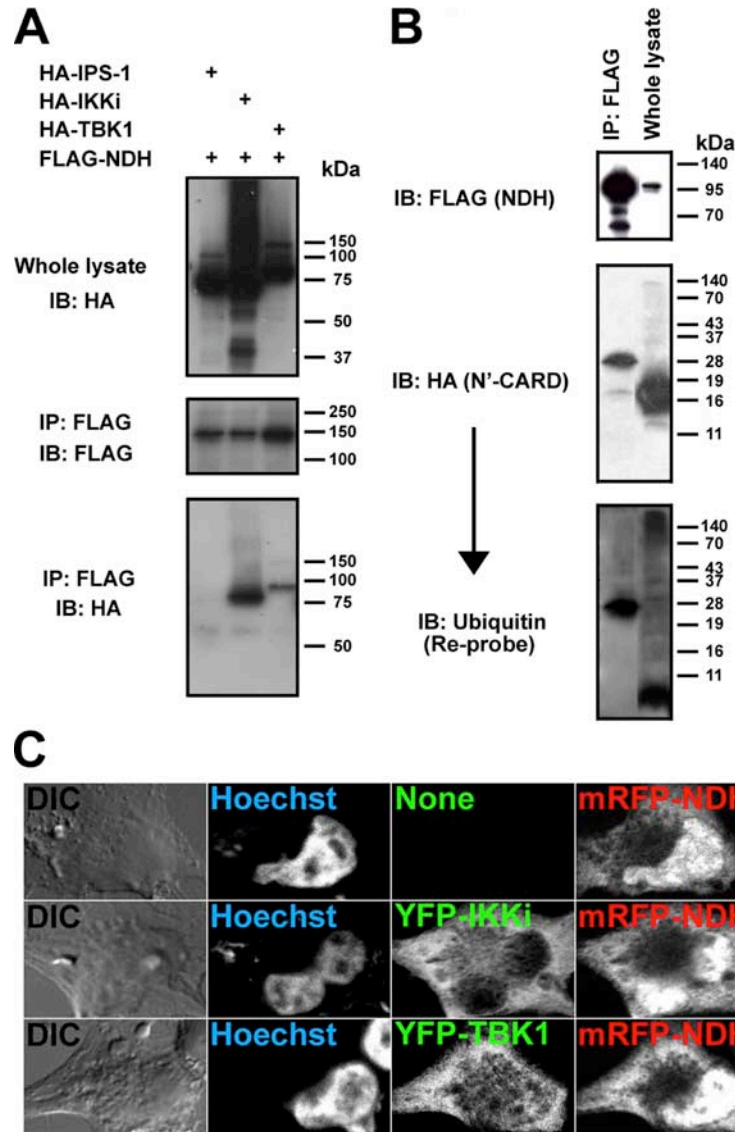


**FIGURE 3.** NDH associates with N'-CARD, TBK1, and IKKi. *A* and *B*, The lysates of HEK293 cells transfected with the expression plasmids for FLAG-NDH plus HA-IPS-1, HA-IKKi, HA-TBK1 (*A*) or N'-CARD-HA (*B*) were prepared and immunoprecipitated with anti-FLAG Ab. The immunoblots were probed with anti-HA or anti-FLAG Ab (*A* and *B*) or sequentially probed with anti-HA and anti-ubiquitin Ab (*B*). *C*, HeLa cells were transfected with an expression plasmid for mRFP-NDH alone or with those for mRFP-NDH and YFP-IKKi or YFP-TBK1. After staining with Hoechst 33258, the cells were examined under a confocal microscope. Data represent one of three independent experiments with similar results. Scale bar, 10  $\mu$ m.

those downstream of IPS-1, and that it plays a role in signaling upstream of TBK1.

To confirm the physical interactions among NDH, IKKi, TBK1, and N'-CARD, immunoprecipitation analysis was performed. A strong interaction was detected between NDH and IKKi or TBK1, while there was no apparent association of NDH with IPS-1 in this assay (Fig. 3*A*). By contrast, NDH was confirmed to interact with N'-CARD. Of interest, the mobility of N'-CARD coprecipitated with NDH was retarded in SDS-PAGE (~25 kDa) when compared with that in whole cell lysate (~18 kDa) (Fig. 3*B*). The retarded N'-CARD was detected by anti-ubiquitin Ab, suggesting that mono-ubiquitinated N'-CARD, directly or indirectly, has the ability to associate with NDH (Fig. 3*B*). We also examined the subcellular localization of NDH, IKKi, and TBK1 by confocal microscopy analysis (Fig. 3*C*). Both YFP-IKKi and YFP-TBK1 were mostly present in the cytoplasm, while mRFP-NDH was diffusely present within the cell. Most NDH present within the cytoplasm colocalized with IKKi or TBK1 (Fig. 3*C*).

*Recombinant N'-CARD polypeptide fused to the protein transduction domain (N'-CARD-PTD) induces type I IFN production and exerts innate immune responses in vitro*

To examine the potent ability of N'-CARD in modulating innate immune responses, we generated a recombinant N'-CARD

polypeptide fused to the PTD, which enables transduction of extracellular protein into intracellular compartments. When the N'-CARD-PTD polypeptide was added to the culture medium of HeLa cells, it entered the nucleus within 30 min (Fig. 4*A*). By contrast, when the same amount of CARD polypeptide was added, only a minimal level of the polypeptide was observed inside the cell (Fig. 4*A*). The addition of the N'-CARD-PTD polypeptide alone induced significant levels of IFN- $\beta$  promoter activation in HEK293 cells, suggesting that N'-CARD-PTD has the ability to translocate into the cell and trigger NDH-mediated cellular signaling to elicit type I IFN production (Supplemental Fig. 2).

We next examined whether administration of the N'-CARD-PTD polypeptide activates immune cells in vitro. As shown in Fig. 4*B*, N'-CARD-PTD induced production of a proinflammatory cytokine (TNF- $\alpha$ ), type I IFNs (IFN- $\alpha$  and - $\beta$ ), and an IFN-stimulated gene product (IP-10) in a mouse macrophage cell line, RAW264.7. The expression of IFN- $\alpha$  and - $\beta$  mRNAs was detected within 18 h; the expression of IFN- $\alpha$  mRNA continued for more than 48 h after N'-CARD-PTD treatment. By contrast, LPS, an activator of TLR4-mediated innate immune responses, induced IFN- $\beta$  mRNA within 3 h, but this induction lasted for less than 18 h. The overall level of IFN- $\alpha$  mRNA production was higher in cells stimulated with N'-CARD-PTD compared with those stimulated with LPS, while that of IFN- $\beta$  was lower in those stimulated

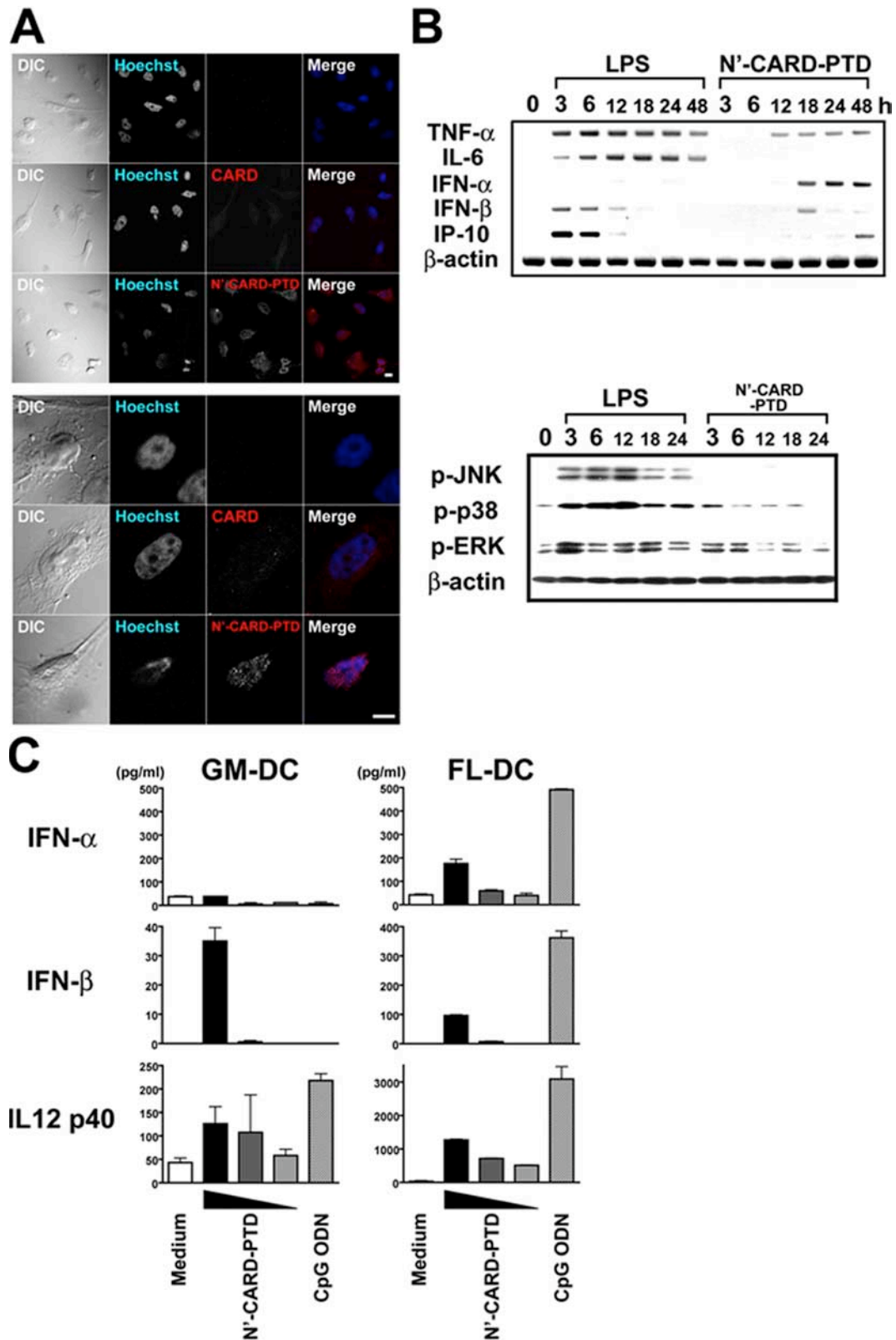


**FIGURE 4.** The N'-CARD-PTD polypeptide induces type I IFN production and DC maturation. *A*, Recombinant CARD or N'-CARD-PTD polypeptide was administered into the culture medium of HeLa cells. Thirty minutes after addition, the cells were permeabilized, stained with anti-FLAG M2-Cy3 and Hoechst 33258, and subjected to confocal microscopy analysis. *Upper panel*, Lower magnification. *Lower panel*, Higher magnification. Scale bar, 10  $\mu$ m. *B*, RAW264.7 cells were treated with 1  $\mu$ g/ml LPS or 10  $\mu$ g/ml N'-CARD-PTD for 3, 6, 12, 18, 24, and 48 h. The levels of mRNA expression for TNF- $\alpha$ , IL-6, IFN- $\alpha$ , IFN- $\beta$ , IP-10 and  $\beta$ -actin were examined by RT-PCR (*upper panel*). The levels of phosphorylated JNK, p38, or ERK were examined by immunoblotting (*lower panel*). *C*, GM-DCs or FL-DCs were treated with or without 1, 3, or 10  $\mu$ g/ml N'-CARD-PTD or 1  $\mu$ M of CpG ODN for 24 h and the supernatants were subjected to ELISA for mouse IFN- $\alpha$ , IFN- $\beta$ , or IL-12 p40. Data represent one of two or three independent experiments with similar results.

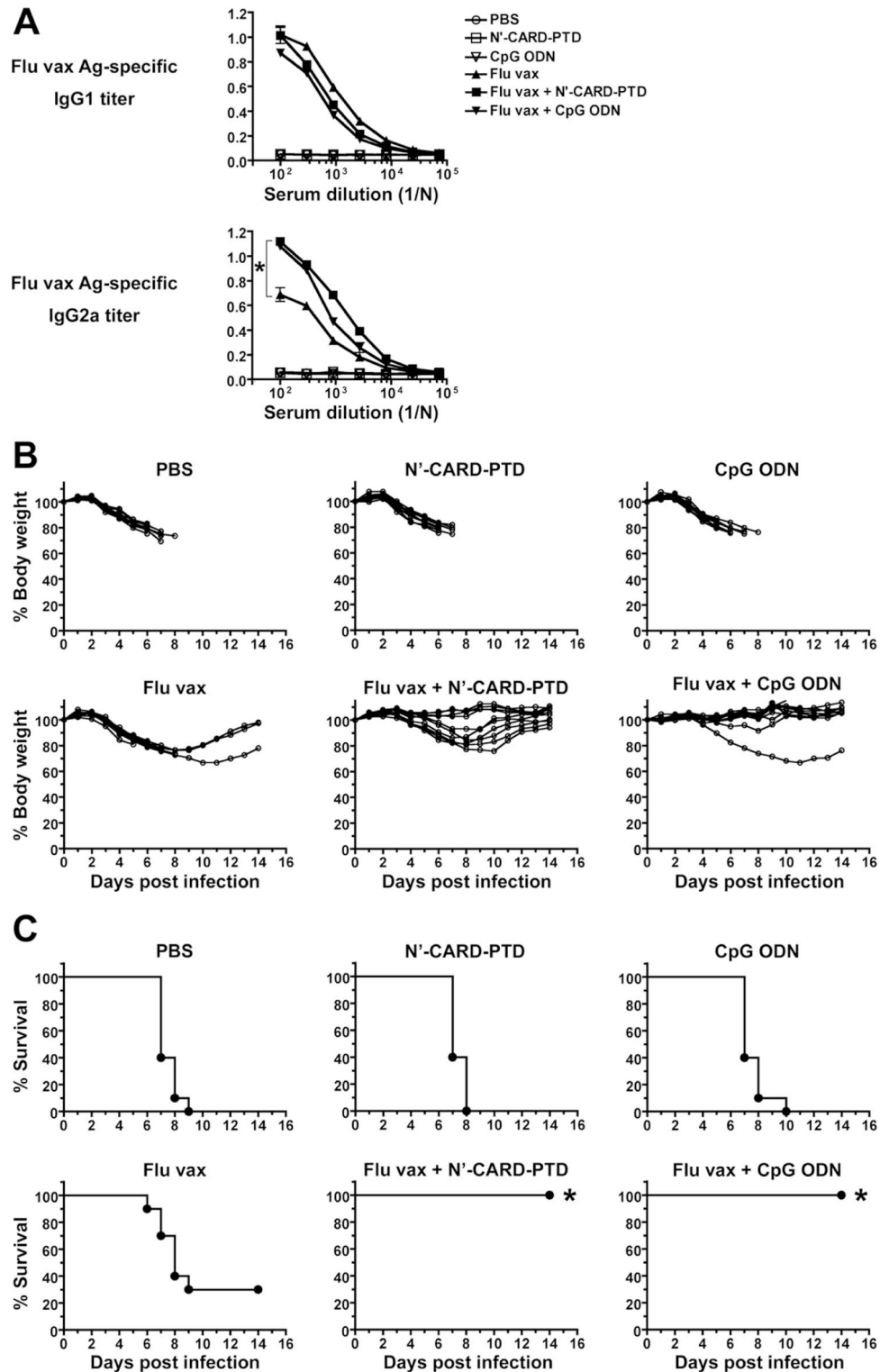
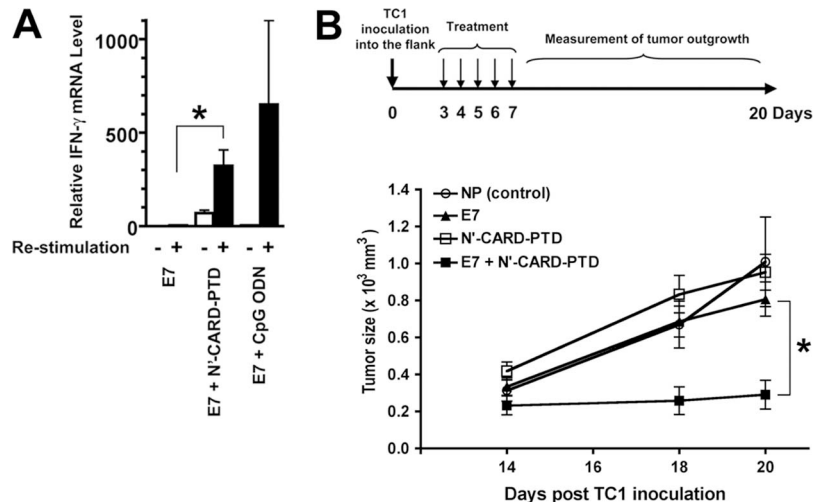


**FIGURE 5.** Coadministration of N'-CARD-PTD enhances Ag-specific IgG2a production and superior protection against lethal influenza infection. A–C, Eight-week-old female BALB/c mice ( $n = 10$ ) were immunized s.c. with flu vax ( $0.7 \mu\text{g}$ ), N'-CARD-PTD ( $5 \mu\text{g}$ ), CpG ODN ( $5 \mu\text{g}$ ), flu vax ( $0.7 \mu\text{g}$ ) plus N'-CARD-PTD ( $5 \mu\text{g}$ ), or flu vax ( $0.7 \mu\text{g}$ ) plus CpG ODN ( $5 \mu\text{g}$ ) at 0 and 10 days. A, Anti-flu vax Ab titer was examined 10 days after the final immunization. B and C, Ten days after the final immunization, mice were challenged with 8 LD<sub>50</sub> doses of influenza A/P/R8 (H1N1). The body-weight changes (B) and the mortality (C) were monitored for the next 14 days. Data represent one of two independent experiments with similar results. \*,  $p < 0.05$ .

with N'-CARD-PTD compared with those stimulated LPS (Fig. 4B). These results suggest that N'-CARD-PTD activates a distinct innate immune signaling pathway(s) from those engaged by LPS. In fact, LPS induced phosphorylation of MAPK such as JNK, p38, and ERK within 3 h, while N'-CARD-PTD had little effects on activation of these kinases except for ERK at 3 and 6 h (Fig. 4B). We also examined whether N'-CARD-PTD activates bone marrow-derived dendritic cells (BM-DCs). As a control, CpG ODN activated BM-DCs induced in vitro by Flt3L (FL-DCs) but not BM-DCs induced in

vitro by GM-CSF (GM-DCs) to produce type I IFNs. N'-CARD-PTD, by contrast, activated both GM-DCs and FL-DCs to produce type I IFNs (Fig. 4C). We also observed that N'-CARD-PTD weakly but significantly up-regulated cell surface expression of MHC class I, class II, CD40, and CD86 on both GM-DCs and FL-DCs (data not shown). Up-regulation of such cell surface molecules was dependent on type I IFN production but independent on myeloid differentiation factor 88 (MyD88) nor Toll-IL-1R domain-containing adaptor-inducing IFN- $\beta$  (TRIF) (data not shown).

**FIGURE 6.** Coadministration of N'-CARD-PTD plus tumor-associated Ag E7 confers superior protection against tumor outgrowth. **A**, Eight-week-old female BALB/c mice ( $n = 5$ ) were immunized subcutaneously with E7 peptide (3  $\mu\text{g}$ ), E7 peptide (3  $\mu\text{g}$ ) plus N'-CARD-PTD (5  $\mu\text{g}$ ), or E7 peptide (3  $\mu\text{g}$ ) plus CpG ODN (5  $\mu\text{g}$ ) at 2 and 4 wk. Splenocytes were prepared from each individual mouse and restimulated in vitro with control NP (-) or E7 peptide ( $\pm$ ). The relative expression levels of IFN- $\gamma$  mRNA were measured by real-time PCR and normalized to 18S rRNA levels. **B**, Eight-week-old C57BL/6 mice ( $n = 10$ ) were inoculated subcutaneously with  $1 \times 10^5$  TC-1 cells/mouse at 0 days and then immunized with control NP peptide (3  $\mu\text{g}$ ), E7 (3  $\mu\text{g}$ ), N'-CARD-PTD (5  $\mu\text{g}$ ), or E7 (3  $\mu\text{g}$ ) plus N'-CARD-PTD (5  $\mu\text{g}$ ) at 3, 4, 5, 6, and 7 days. Tumor sizes were measured at 14, 18, and 20 days. Data represent one of two independent experiments with similar results. \*,  $p < 0.01$ .



### N'-CARD-PTD augments Ag-specific acquired immune responses to protect against influenza virus infection and tumor outgrowth in vivo

To examine the in vivo effects of N'-CARD-PTD on innate and acquired immune responses, we used a mouse model of influenza virus infection and of tumor transplantation. Influenza split-product vaccine (flu vax) was used to evaluate the adjuvanticity of N'-CARD-PTD. Flu vax was prepared at The Research Foundation for Microbial Diseases of Osaka University from the purified influenza virus A/New Caledonia/20/99 strain treated sequentially with ether and formalin. As shown in Fig. 5A, s.c. administration of flu vax plus N'-CARD-PTD or CpG ODN induced significant levels of specific IgG1 production that were comparable to that of flu vax alone. Administration of flu vax plus N'-CARD-PTD or CpG ODN, by contrast, resulted in significantly higher levels of specific IgG2a production compared with that of flu vax alone, suggesting that N'-CARD-PTD and CpG ODN have the ability to modulate Th1-deviated immune responses. In accordance with such adjuvant effects, immunization with flu vax plus N'-CARD-PTD conferred superior protection against a lethal influenza challenge relative to that with flu vax alone (Fig. 5, B and C).

We next examined whether N'-CARD-PTD has an ability to enhance Ag-specific cellular immune responses. Immunization with MHC class I-restricted HPV E7 peptide (E7) alone induced minimal levels of E7-specific IFN- $\gamma$  production from splenocytes (Fig. 6A). Treatment with E7 plus N'-CARD-PTD or CpG ODN induced higher levels of E7-specific IFN- $\gamma$  production, suggesting that N'-CARD-PTD has an adjuvant effect on cell-mediated immune responses (Fig. 6A). Thus, mice were s.c. transplanted with TC-1 cells expressing E7 as a model tumor Ag, and then immunized with E7 in the presence or absence of N'-CARD-PTD, as shown in Fig. 6B. The outgrowth of TC-1 tumors in mice treated with either N'-CARD-PTD or E7 alone was comparable to that in mice treated with control NP peptide. In accordance with E7-specific IFN- $\gamma$  production from splenocytes, the sizes of established tumors in mice treated with E7 plus N'-CARD-PTD were significantly smaller compared with those in mice treated with E7 alone or with N'-CARD-PTD alone (Fig. 6B). These in vivo results, taken together, indicate that N'-CARD-PTD, an activator of NDH-mediated innate immune responses, acts as a vaccine adjuvant, thereby enhancing protective immune responses against pathogens or tumors.

### Discussion

This study provides the first evidence that the N'-CARD-PTD polypeptide directly enters the nucleus and triggers the innate immune signaling pathway leading to type I IFN production through NDH. NDH is a member of the DEXH (Asp-Glu-X-His) family of helicases and is highly conserved in higher eukaryotes, from *Drosophila* to mammals. Previous studies have shown that NDH interacts with molecules of the transcription machinery, such as the RNA polymerase II complex (28), cAMP-response element-binding protein (28), and NF- $\kappa$ B p65 (29), thereby regulating the transcription of responsive genes. NDH also acts together with the RNA editing enzyme to coordinate the editing and splicing of numerous cellular and viral RNAs (30, 31). Knockout of the *Ndh* gene led to early embryonic lethality (<E10.5) due to a high frequency of apoptosis in embryonic ectodermal cells during gastrulation (32). In addition to these properties of gene regulation and cellular homeostasis, our results suggest that NDH has a distinct property of mediating innate immune signaling upstream of TBK1. Recently, it was shown that a DEAD (Asp-Glu-Ala-Asp) box helicase, DDX3X, is a kinase substrate of TBK1 and acts as a critical component of TBK1-dependent innate immune signaling, particularly in the type I IFN production pathway (33).

MAPK activation plays a significant role in LPS- or CpG DNA-mediated signaling (Fig. 4C and Ref. 34), however, the signaling pathway induced by N'-CARD-PTD may not involve MAPK. This suggested that, unlike TLR-mediated signaling pathways, activation of MAPK is not crucial for N'-CARD-PTD-mediated type I IFN production. Rather, the action of N'-CARD-PTD resembles the signal activation induced by IFN stimulatory DNA, which was originally reported by Stetson et al. as having a similar action to B-DNA, which is critical in the control of DNA vaccine immunogenicity (5, 35). Because MAPK activation is associated with deleterious effects, ranging from hyperinflammation to cancer (36), the lack of such kinase activation would be an advantage for the repeated clinical application of N'-CARD-PTD. Further study will be needed to elucidate the molecular basis of the NDH-mediated signaling pathway and to determine the value of N'-CARD-PTD for clinical use.

Many TLR ligands and related compounds have been tested as vaccine adjuvants and as anti-allergy and anti-cancer drugs in humans (37). Among these, some clinical trials of TLR9-targeting molecules, including CpG ODN and its conjugated products, have recently been abandoned due to unexpectedly weaker responses in

humans relative to those observed in mice. This result was attributable to a lower frequency of TLR9 expression in human immune cells; expression was found in only a portion of B cells and plasmacytoid DCs that combined made up just 1% of the total immune cell population (38). In contrast, immunostimulatory RNA or B-DNA activates innate immune responses through cytosolic receptors but only when they are introduced into intracellular compartments, i.e., they have almost no effects when they are present outside the cell. Taking such observations into account, N'-CARD-PTD may have the advantage of self-transmigration into the nucleus and of triggering innate immune signaling in the absence of TLRs but in the presence of NDH and TBK1, which are ubiquitously expressed in a wide-variety of cell types.

In conclusion, this study showed concrete evidence that the activation of a distinct NDH-mediated signaling pathway up-regulates innate immune responses and that N'-CARD-PTD is a candidate vaccine adjuvant in future vaccine development. These findings may also provide insights that will be helpful in the design of immunomodulatory agents, such as using constitutively active signaling molecules of the innate immune responses.

## Disclosures

The authors have no financial conflict of interest.

## References

- Barr, S. D., J. R. Smiley, and F. D. Bushman. 2008. The interferon response inhibits HIV particle production by induction of TRIM22. *PLoS Pathog.* 4: 1–11.
- Fodil-Cornu, N., and S. M. Vidal. 2008. Type I interferon response to cytomegalovirus infection: the kick-start. *Cell Host Microbes* 3: 59–61.
- Bracci, L., E. Proietti, and F. Belardelli. 2007. IFN- $\alpha$  and novel strategies of combination therapy for cancer. *Ann. NY Acad. Sci.* 1112: 256–268.
- Ferrantini, M., I. Capone, and F. Belardelli. 2007. Interferon- $\alpha$  and cancer: mechanisms of action and new perspectives of clinical use. *Biochimie* 89: 884–893.
- Ishii, K. J., T. Kawagoe, S. Koyama, K. Matsui, H. Kumar, T. Kawai, S. Uematsu, O. Takeuchi, F. Takeshita, C. Coban, and S. Akira. 2008. TANK-binding kinase-1 delineates innate and adaptive immune responses to DNA vaccines. *Nature* 451: 725–729.
- Ishii, K. J., C. Coban, H. Kato, K. Takahashi, Y. Torii, F. Takeshita, H. Ludwig, G. Sutter, K. Suzuki, H. Hemmi, et al. 2006. A Toll-like receptor-independent antiviral response induced by double-stranded B-form DNA. *Nat. Immunol.* 7: 40–48.
- Zhu, J., X. Huang, and Y. Yang. 2007. Innate immune response to adenoviral vectors is mediated by both Toll-like receptor-dependent and -independent pathways. *J. Virol.* 81: 3170–3180.
- Takeuchi, O., and S. Akira. 2008. MDA5/RIG-I and virus recognition. *Curr. Opin. Immunol.* 20: 17–22.
- Kawai, T., and S. Akira. 2007. Antiviral signaling through pattern recognition receptors. *J. Biochem.* 141: 137–145.
- Yoshida, H., Y. Okabe, K. Kawane, H. Fukuyama, and S. Nagata. 2005. Lethal anemia caused by interferon- $\beta$  produced in mouse embryos carrying undigested DNA. *Nat. Immunol.* 6: 49–56.
- Kawane, K., M. Ohtani, K. Miwa, T. Kizawa, Y. Kanbara, Y. Yoshioka, H. Yoshikawa, and S. Nagata. 2006. Chronic polyarthritis caused by mammalian DNA that escapes from degradation in macrophages. *Nature* 443: 998–1002.
- Kato, H., O. Takeuchi, S. Sato, M. Yoneyama, M. Yamamoto, K. Matsui, S. Uematsu, A. Jung, T. Kawai, K. J. Ishii, et al. 2006. Differential roles of MDA5 and RIG-I helicases in the recognition of RNA viruses. *Nature* 441: 101–105.
- Cheng, G., J. Zhong, J. Chung, and F. V. Chisari. 2007. Double-stranded DNA and double-stranded RNA induce a common antiviral signaling pathway in human cells. *Proc. Natl. Acad. Sci. USA* 104: 9035–9040.
- Takahashi, K., M. Yoneyama, T. Nishihori, R. Hirai, H. Kumeta, R. Narita, M. Gale, Jr., F. Inagaki, and T. Fujita. 2008. Nonself RNA-sensing mechanism of RIG-I helicase and activation of antiviral immune responses. *Mol. Cell* 29: 428–440.
- Ishii, K. J., S. Koyama, A. Nakagawa, C. Coban, and S. Akira. 2008. Host innate immune receptors and beyond: making sense of microbial infections. *Cell Host Microbes* 3: 352–363.
- Potter, J. A., R. E. Randall, and G. L. Taylor. 2008. Crystal structure of human IPS-1/MAVS/VISA/Cardif caspase activation recruitment domain. *BMC Struct. Biol.* 8: 11.
- Loo, Y. M., D. M. Owen, K. Li, A. K. Erickson, C. L. Johnson, P. M. Fish, D. S. Carney, T. Wang, H. Ishida, M. Yoneyama, et al. 2006. Viral and therapeutic control of IFN- $\beta$  promoter stimulator 1 during hepatitis C virus infection. *Proc. Natl. Acad. Sci. USA* 103: 6001–6006.
- Sung, M., G. M. Poon, and J. Gariepy. 2006. The importance of valency in enhancing the import and cell routing potential of protein transduction domain-containing molecules. *Biochim. Biophys. Acta* 1758: 355–363.
- Davenport, F. M., A. V. Hennessy, F. M. Brandon, R. G. Webster, C. D. Barrett, Jr., and G. O. Lease. 1964. Comparisons of serologic and febrile responses in humans to vaccination with influenza A viruses or their hemagglutinins. *J. Lab. Clin. Med.* 63: 5–13.
- Tanimoto, T., R. Nakatsu, I. Fuke, T. Ishikawa, M. Ishibashi, K. Yamanishi, M. Takahashi, and S. Tamura. 2005. Estimation of the neuraminidase content of influenza viruses and split-product vaccines by immunochromatography. *Vaccine* 23: 4598–4609.
- Kawai, T., K. Takahashi, S. Sato, C. Coban, H. Kumar, H. Kato, K. J. Ishii, O. Takeuchi, and S. Akira. 2005. IPS-1, an adaptor triggering RIG-I- and Mda5-mediated type I interferon induction. *Nat. Immunol.* 6: 981–988.
- Jounai, N., F. Takeshita, K. Kobiyama, A. Sawano, A. Miyawaki, K. Q. Xin, K. J. Ishii, T. Kawai, S. Akira, K. Suzuki, and K. Okuda. 2007. The Atg5 Atg12 conjugate associates with innate antiviral immune responses. *Proc. Natl. Acad. Sci. USA* 104: 14050–14055.
- Takeshita, F., K. Suzuki, S. Sasaki, N. Ishii, D. M. Klinman, and K. J. Ishii. 2004. Transcriptional regulation of the human TLR9 gene. *J. Immunol.* 173: 2552–2561.
- Takeshita, F., K. J. Ishii, K. Kobiyama, Y. Kojima, C. Coban, S. Sasaki, N. Ishii, D. M. Klinman, K. Okuda, S. Akira, and K. Suzuki. 2005. TRAF4 acts as a silencer in TLR-mediated signaling through the association with TRAF6 and TRIF. *Eur. J. Immunol.* 35: 2477–2485.
- Takeshita, F., T. Tanaka, T. Matsuda, M. Tozuka, K. Kobiyama, S. Saha, K. Matsui, K. J. Ishii, C. Coban, S. Akira, et al. 2006. Toll-like receptor adaptor molecules enhance DNA-raised adaptive immune responses against influenza and tumors through activation of innate immunity. *J. Virol.* 80: 6218–6224.
- Seth, R. B., L. Sun, C. K. Ea, and Z. J. Chen. 2005. Identification and characterization of MAVS, a mitochondrial antiviral signaling protein that activates NF- $\kappa$ B and IRF 3. *Cell* 122: 669–682.
- Fitzgerald, K. A., S. M. McWhirter, K. L. Faia, D. C. Rowe, E. Latz, D. T. Golenbock, A. J. Coyle, S. M. Liao, and T. Maniatis. 2003. IKK $\epsilon$  and TBK1 are essential components of the IRF3 signaling pathway. *Nat. Immunol.* 4: 491–496.
- Nakajima, T., C. Uchida, S. F. Anderson, C. G. Lee, J. Hurwitz, J. D. Parvin, and M. Montminy. 1997. RNA helicase A mediates association of CBP with RNA polymerase II. *Cell* 90: 1107–1112.
- Tetsuka, T., H. Uranishi, T. Sanda, K. Asamitsu, J. P. Yang, F. Wong-Staal, and T. Okamoto. 2004. RNA helicase A interacts with nuclear factor  $\kappa$ B p65 and functions as a transcriptional coactivator. *Eur. J. Biochem.* 271: 3741–3751.
- Bratt, E., and M. Ohman. 2003. Coordination of editing and splicing of glutamate receptor pre-mRNA. *RNA* 9: 309–318.
- Maas, S., A. Rich, and K. Nishikura. 2003. A-to-I RNA editing: recent news and residual mysteries. *J. Biol. Chem.* 278: 1391–1394.
- Lee, C. G., V. da Costa Soares, C. Newberger, K. Manova, E. Lacy, and J. Hurwitz. 1998. RNA helicase A is essential for normal gastrulation. *Proc. Natl. Acad. Sci. USA* 95: 13709–13713.
- Soulat, D., T. Burckstummer, S. Westermayer, A. Goncalves, A. Bauch, A. Stefanovic, O. Hantschel, K. L. Bennett, T. Decker, and G. Superti-Furga. 2008. The DEAD-box helicase DDX3X is a critical component of the TANK-binding kinase 1-dependent innate immune response. *EMBO J.* 27: 2135–2146.
- Hacker, H., H. Mischak, G. Hacker, S. Eser, N. Prenzel, A. Ullrich, and H. Wagner. 1999. Cell type-specific activation of mitogen-activated protein kinases by CpG-DNA controls interleukin-12 release from antigen-presenting cells. *EMBO J.* 18: 6973–6982.
- Stetson, D. B., and R. Medzhitov. 2006. Recognition of cytosolic DNA activates an IRF3-dependent innate immune response. *Immunity* 24: 93–103.
- Salh, B. 2007. c-Jun N-terminal kinases as potential therapeutic targets. *Expert Opin. Ther. Targets.* 11: 1339–1353.
- Kanzler, H., F. J. Barrat, E. M. Hessel, and R. L. Coffman. 2007. Therapeutic targeting of innate immunity with Toll-like receptor agonists and antagonists. *Nat. Med.* 13: 552–559.
- Schmidt, C. 2007. Clinical setbacks for Toll-like receptor 9 agonists in cancer. *Nat. Biotechnol.* 25: 825–826.

# The IFITM Proteins Mediate Cellular Resistance to Influenza A H1N1 Virus, West Nile Virus, and Dengue Virus

Abraham L. Brass,<sup>1,2,4,9,\*</sup> I-Chueh Huang,<sup>5,9</sup> Yair Benita,<sup>3,10</sup> Sinu P. John,<sup>1,10</sup> Manoj N. Krishnan,<sup>6</sup> Eric M. Feeley,<sup>1</sup> Bethany J. Ryan,<sup>1</sup> Jessica L. Weyer,<sup>5</sup> Louise van der Weyden,<sup>8</sup> Erol Fikrig,<sup>6,7</sup> David J. Adams,<sup>8</sup> Ramnik J. Xavier,<sup>2,3</sup> Michael Farzan,<sup>5,\*</sup> and Stephen J. Elledge<sup>4,\*</sup>

<sup>1</sup>Ragon Institute of Massachusetts General Hospital, Massachusetts Institute of Technology, and Harvard Medical School, Charlestown, MA 02129, USA

<sup>2</sup>Gastrointestinal Unit

<sup>3</sup>Center for Computational and Integrative Biology

Massachusetts General Hospital, Harvard Medical School, Boston, MA 02114, USA

<sup>4</sup>Department of Genetics, Harvard Medical School, Division of Genetics, Brigham and Women's Hospital,

Howard Hughes Medical Institute, Boston, MA 02115, USA

<sup>5</sup>Department of Microbiology and Molecular Genetics, Harvard Medical School, New England Primate Research Center, Southborough, MA 01772, USA

<sup>6</sup>Section of Infectious Diseases, Department of Internal Medicine

<sup>7</sup>Howard Hughes Medical Institute

Yale University School of Medicine, New Haven, CT 06520, USA

<sup>8</sup>Experimental Cancer Genetics, Wellcome Trust Sanger Institute, Wellcome Trust Genome Campus, Hinxton Cambridge CB10 1SA, UK

<sup>9</sup>These authors contributed equally to this work

<sup>10</sup>These authors contributed equally to this work

\*Correspondence: [abrass@partners.org](mailto:abrass@partners.org) (A.L.B.), [farzan@hms.harvard.edu](mailto:farzan@hms.harvard.edu) (M.F.), [selledge@genetics.med.harvard.edu](mailto:selledge@genetics.med.harvard.edu) (S.J.E.)

DOI 10.1016/j.cell.2009.12.017

## SUMMARY

Influenza viruses exploit host cell machinery to replicate, resulting in epidemics of respiratory illness. In turn, the host expresses antiviral restriction factors to defend against infection. To find host cell modifiers of influenza A H1N1 viral infection, we used a functional genomic screen and identified over 120 influenza A virus-dependency factors with roles in endosomal acidification, vesicular trafficking, mitochondrial metabolism, and RNA splicing. We discovered that the interferon-inducible transmembrane proteins IFITM1, 2, and 3 restrict an early step in influenza A viral replication. The IFITM proteins confer basal resistance to influenza A virus but are also inducible by interferons type I and II and are critical for interferon's virustatic actions. Further characterization revealed that the IFITM proteins inhibit the early replication of flaviviruses, including dengue virus and West Nile virus. Collectively this work identifies a family of antiviral restriction factors that mediate cellular innate immunity to at least three major human pathogens.

## INTRODUCTION

Influenza epidemics exact a formidable toll on world health. Moreover, viral super-infections can produce antigenic shifting,

resulting in more virulent pathogens (Monto, 2009). At present, the emergence of a novel influenza A H1N1 viral strain has created a pandemic, producing illness in over 200 countries and territories (World Health Organization Pandemic [H1N1] 2009—update 75). Additionally, the related avian influenza A viral strain, H5N1, represents a potentially catastrophic global health risk (Maines et al., 2008).

The influenza A viral genome encodes for 11 proteins and consists of 8 segments of negative single-stranded RNA (Lamb and Krug, 2001). Each subgenomic segment is coated by viral nucleoprotein (NP) and bound to a single viral RNA-dependent RNA-polymerase holoenzyme (RdRp), composed of PA, PB1, and PB2 subunits. Infection begins with the binding of the viral hemagglutinin (HA) protein to sialylated host cell-surface glycoproteins (Skehel and Wiley, 1995). Following endocytosis, viral particles are trafficked through both early and late endosomes, with the acidification of the latter compartment altering the conformation of HA, leading to host-viral membrane fusion, entry of the viral ribonucleoproteins (vRNPs) into the cytosol (Sieczkarski and Whittaker, 2003), and nuclear import.

Once in the nucleus, the RdRp commandeers 5' caps from host mRNAs to prime transcription of viral mRNA (vmRNA; Bouloy et al., 1978) and creates positive sense complementary RNA (cRNA) from which it makes new viral genomes (vRNAs). The vRNAs are coated by NP and exported through the nuclear pore complex (NPC) by the viral factors M1 and NEP/NS2 (nuclear export protein) working in concert with the host nuclear export machinery. The viral envelope proteins HA, M2, and neuraminidase (NA) are translated on the rough endoplasmic reticulum (ER) and trafficked to the cell surface where they, along with

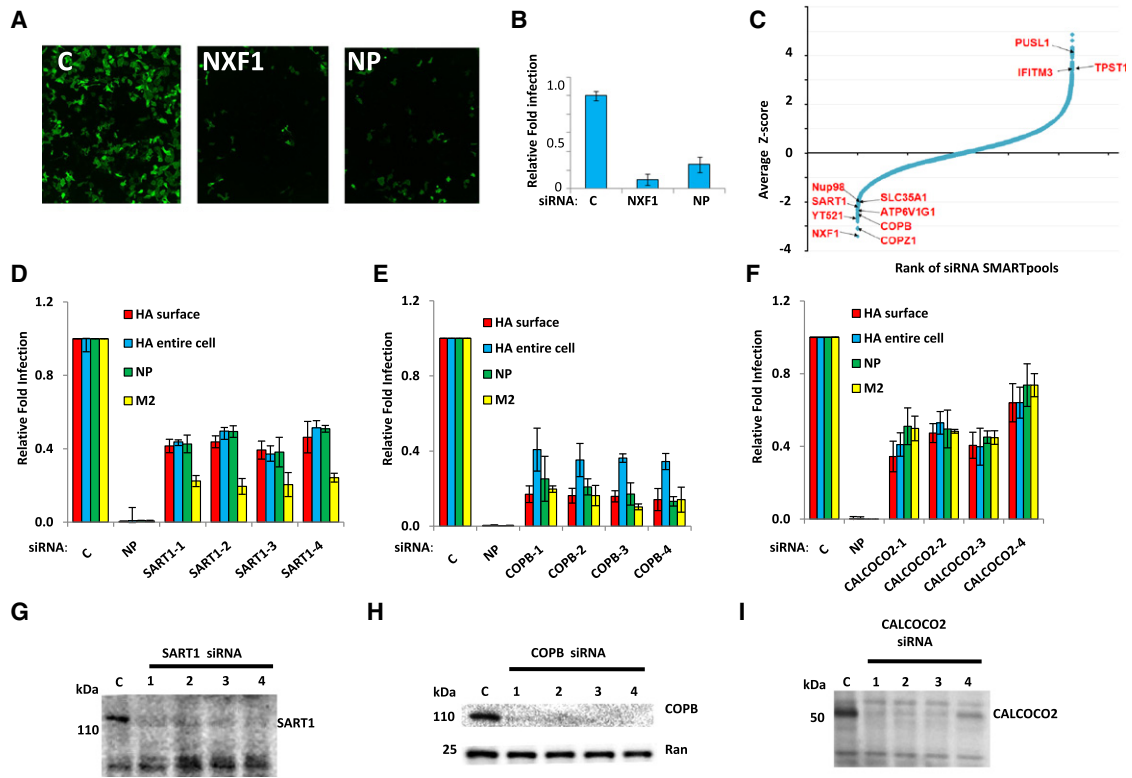


**Figure 1. The siRNA Screen for Influenza A Virus Infection-Modifying Host Factors**

(A) U2OS cells were transfected with the indicated siRNAs, then infected with influenza A virus (PR8) and immunostained 12 hr later for hemagglutinin (HA, green). NP, siRNA targeting flu nucleoprotein; C, nontargeting siRNA negative control. Magnification, 4x.

(B) Quantification of samples in (A). Relative fold infection is normalized to nontargeting (C) control. Values represent the mean  $\pm$  standard deviation (SD), n = 4.

(C) The results of the screen are shown with the siRNA SMARTpools ranked in order of average Z score, from lowest (decreased infection) to highest (increased infection). The position of known influenza A virus-host factors and several newly identified genes from the screen are indicated.

(D–F) U2OS cells were transfected with the indicated siRNAs for 72 hr, then infected with PR8. Twelve hours after infection the cells were analyzed by IF for the following viral proteins, HA (surface or entire cell), NP, and M2. Relative fold infection is normalized to nontargeting (C) control. Values represent the mean  $\pm$  SD, n = 4.

(G–I) Western blots for cells in (D)–(F). C, nontargeting siRNA negative control. Ran levels are provided to demonstrate relative protein loading when cross-reacting bands were not present.

the soluble factors M1, RdRp, and eight distinct vRNPs, are packaged into budding virions.

To defend against infection, the host mobilizes factors to confront the virus. Interferons (IFN) orchestrate a large component of this antiviral response (Takaoka and Yanai, 2006). Over 2000 gene products are induced after IFN stimulation, including the antiviral effectors MxA, PKR, RIG-I, and 2'5'-OAS (Haller et al., 2009; Nakhaei et al., 2009; Takaoka and Yanai, 2006). However, many viruses deploy anti-IFN countermeasures, which for influenza A virus are primarily enacted by the viral protein NS1 (Hale et al., 2008). To identify host factors that modify viral replication we undertook an siRNA screen. In this screen we identified over 120 host factors required for influenza A replication that identify many central functions and interactions required for the viral life cycle as well as potential antiviral drug targets. Our studies also revealed a family of antiviral factors, the IFITM proteins, that mediate interferon's innate immune role in combating not only all pathogenic influenza A virus strains examined but also West Nile virus and dengue virus.

**RESULTS**

**An siRNA Screen for Influenza A Virus Infection-Modifying Host Factors**

We used a single round infection screen of osteosarcoma cells (U2OS) to find host proteins that modify the life cycle of influenza A virus A/Puerto Rico/8/34 H1N1 (PR8). After 12 hr the cells were stained for surface expression of HA as an indirect surrogate marker for viral infection (Figure 1A). Although measuring viral protein levels is an indirect measurement of viral replication, in three previous viral screens where we measured HIV, West Nile virus, and HCV replication by immunofluorescence and by titering, the viral protein reduction strongly correlated with reduction in viral titers. Thus we feel that this indirect assay can provide an accurate measurement of viral impairment. This approach detects viral-host receptor binding, endocytosis and fusion of the virion, vRNP trafficking and nuclear import, the transcription, nuclear export, and translation of the viral HA mRNA, and the trafficking of HA to the surface. The screen

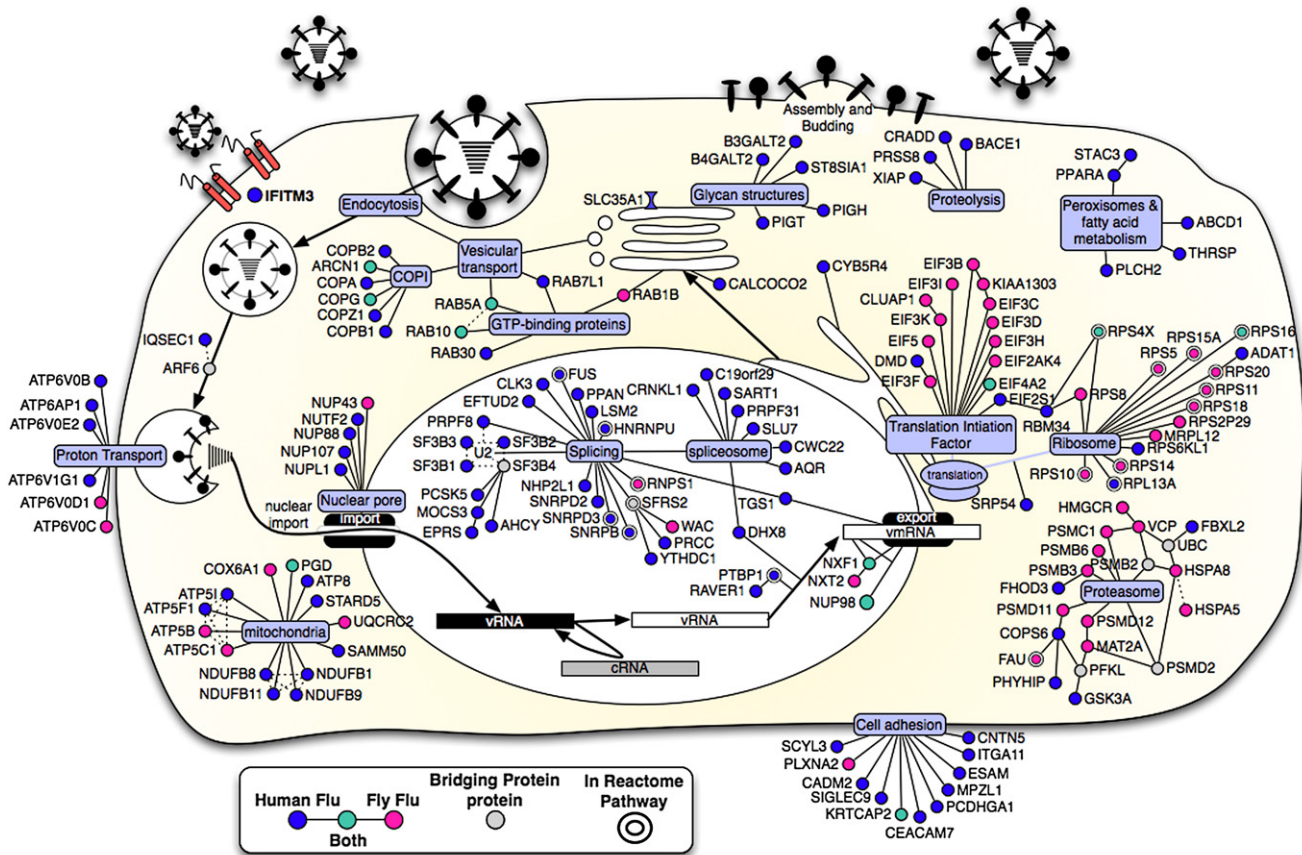


**Figure 2. Integrated Model of Influenza A Virus Host Factors**

Using the influenza A virus life cycle as a guide (Lamb and Krug, 2001), the candidate proteins from the human and fly screens were placed at the position most likely to be relevant to the virus using a database of annotations from Gene Ontology, KEGG, Reactome, and OMIM (see [Experimental Procedures](#)). Computational mapping and supporting evidences were reviewed and refined manually (Datasets S1C–S1F). The known molecular functions of the host factors were determined with the use of bioinformatics and multiple datasets (gray ovals). Host factors identified in the human siRNA screen (blue), the human orthologs of proteins identified in the fly-based screen (pink), factors that were found in both human and fly screens (green), and bridging proteins that were not detected but none-the-less generate potentially insightful interactions (gray) are shown. Double borders signify that the candidate is present in the Reactome influenza A virus infection pathway (Vastrik et al., 2007). Solid lines between genes indicate a protein interaction in human or other species. Dotted lines indicate inferred interaction from literature or annotation. Viral RNA (vRNA), viral complementary RNA (cRNA).

was optimized using siRNAs against NP and the host factor NXF1, an mRNA exporter required for virus replication (Ge et al., 2003; Hao et al., 2008). siRNAs against either NP or NXF1 resulted in inhibition of infection (NXF1 10-fold, NP 4- to 6-fold, [Figures 1A and 1B](#) and [Figure S1A](#) available online).

We screened the Dharmacon siRNA library in triplicate. siRNA pools were selected for further evaluation if the percentage of HA-positive cells was less than 55% of the plate mean, and cell numbers were not less than 40% of the plate mean. These criteria were fulfilled by 312 pools (1.7% of the total genes screened, [Figure 1C](#)). Pools that increased HA expression >200% of the plate mean were also selected for validation (22 pools, 0.1%). We next rescreened the four unique siRNAs from each pool separately. In this screen, 260 out of 334 total pools confirmed with at least one siRNA scoring and 133 confirmed with two or more siRNAs (40%), reducing the probability of off-target effects (Datasets S1A and S1B). We employed bioinformatics to identify networks and enriched gene sets within

this gene set (Dataset S1C). Ninety-two gene ontology (GO) biological process terms, assigned to 109 genes, were significantly enriched (Dataset S2). Of these, 17 are nonredundant and assigned to less than 500 genes, suggesting that they are informative and specific. The most significant terms include RNA splicing (22 genes,  $p = 2e-12$ ), proton transport (7 genes,  $p = 2e-5$ ), and mRNA transport (4 genes,  $p = 9e-3$ , [Figure S1B](#)). Analysis of GO molecular functions identified enrichment for 60 statistically significant terms assigned to 152 genes. Twelve terms were nonredundant and assigned to less than 500 human genes. The most significant terms include RNA binding (15 genes,  $p = 0.014$ ), ATPase activity (6 genes,  $p = 0.008$ ), and NADH dehydrogenase activity (4 genes,  $p = 0.016$ ).

Multiple biological pathways and complexes were also detected, concordant with known elements of the viral life cycle ([Figure 2](#)). Influenza A viral infection depends on sialic acid (SA) residues on the host cell surface, and we found that depletion of the SA transporter, SLC35A1, decreased infection. Our screen

confirmed the functional role of two small GTPases, RAB5A (surface internalization to early endosome trafficking) and RAB7L1 (late endosome trafficking), for viral infection (Sieczkowski and Whittaker, 2003). We also found that lowering RAB10 levels inhibited infection (Hao et al., 2008). RAB10 regulates the movement of endosomes generated from endocytosis downstream of RAB5 (Glodowski et al., 2007). Loss of each of four subunits of the multimeric vacuolar-ATPase proton pump (e.g., ATP6AP1, ATP6V0B, ATP6V1G1, ATP6V0E2) impeded infection, consistent with the low pH needed for fusion. Once released from the endosome, the vRNPs are transported into the nucleus through the NPC (Boulo et al., 2007), and multiple NPC factors were found in the screen.

Several splicing complexes were needed for viral HA protein surface expression, including three components of the U2 small nuclear RNP (snRNP), SF3B1, 2, and 3, and the U2 snRNP-interacting proteins, PRPF8, PTBP1, and FUS (Figure 2; Datasets S1A and S1C). The U4/U6.U5 tri-snRNP, including SART1, was also required (Stevens et al., 2001). Four out of four siRNAs targeting SART1 resulted in lower levels of HA (surface-expressed and total protein), NP, and M2 proteins (Figures 1D and 1G). The decreased levels of all three viral proteins, products of both spliced (M2) and unspliced (HA, NP) messages, suggests a general block in viral protein production with loss of SART1, perhaps secondary to effects on host protein expression.

The vesicular transport complex, coatamer 1 (COP1), scored with multiple components ( $p$  value =  $1e-7$ ). COPI directs both retrograde intra-Golgi and Golgi-to-ER transport (Cai et al., 2007). Depletion of six of seven components of COPI (ARCN1, COPA, COBP1, COBP2, COPG, and COPZ1) inhibited HA surface expression, perhaps by interfering with secretion of the host cell receptor(s) and/or trafficking of HA protein to the cell surface. Although COBP1 siRNAs decreased NP and M2 protein levels, they had a greater effect on surface-expressed versus total HA levels, suggesting that less HA arriving at the cell surface was partly responsible for the phenotype (Figures 1E and 1H). CALCOCO2 (NDP52) was also required for infection (Figures 1F and 1I). CALCOCO2 localizes to the Golgi and interacts with the host proteins, TR6BP and Myosin VI, and may function in regulating secretion (Morriswood et al., 2007).

### Identification of IFITM3 as an Influenza A Virus Restriction Factor

In the validation round, the depletion of four genes, interferon-inducible transmembrane protein 3 (IFITM3), PUSL1, TPST1, and WDR33, resulted in increased viral infection with two or more siRNAs (Dataset S1B). We focused on IFITM3 because of its link to interferon (Friedman et al., 1984). Eight out of eleven distinct siRNAs targeting IFITM3 increased infection, with the levels of knockdown correlating with the phenotype (Figures 3A, 3B, and S3A; Dataset S1B). Increased influenza A virus infection was also observed in primary lung fibroblasts after IFITM3 depletion (Figure S3B) and in HeLa cells (Figures S3C and S3E), with newly budded virus from HeLa cells increased >5 fold in titrating assays (Figure S3D). Lowering IFITM3 levels similarly increased infection by the influenza A H1N1 viral strain WS/33 (Figure 3I) but had no effect on HIV infection (Figure S3F). Stable expression of a C-terminal HA-tagged protein, IFITM3-

HA<sup>6R</sup>, lacking the 3'-untranslated region targeted by siRNA IFITM3-6 rescued resistance to the virus (Figures 3D and 3E). Thus, IFITM3 is required for basal levels of cellular resistance to influenza A virus infection.

The mRNAs for IFITM3, and the closely related and linked genes IFITM1 and 2 (70% and 91% amino acid identity, respectively, Figure S6), are inducible by both IFN types I ( $\alpha$ ) and II ( $\gamma$ ) (Friedman et al., 1984; Lewin et al., 1991), which we confirmed by immunofluorescence (IF) and western blot (Figures 3C and 3F). In unstimulated cells, the majority of IFITM3 resides in the ER (based on colocalization with SA and N-acetylglucosamine-conjugated proteins stained by wheat germ agglutinin, WGA; Figure S3G). IFN exposure, in contrast, triggers the distribution of IFITM3 in a vesicular pattern throughout the cell (Figures 3C, S3H, S3I, and S5D).

### IFITM3 Is Required for Interferon's Antiviral Activity against Influenza A Virus

In view of these dynamic changes, we examined IFITM3's functional role in the IFN response. Either IFN- $\alpha$  or - $\gamma$  strongly decreased basal levels of influenza A virus infection in both U2OS and HeLa cells (Figures 3G, 3H, S4A, and S4B). The depletion of IFITM3 profoundly decreased the antiviral actions of either IFN- $\gamma$  or - $\alpha$  (Figures 3G, 3H, S4A, and S4B), but the inhibition was restored with the stable expression of IFITM3-HA<sup>6R</sup> (Figure 3H). Thus we conclude that IFITM3 is required both for basal levels of resistance as well as for the heightened defenses elicited by IFN- $\gamma$  and - $\alpha$ .

### IFITM1, IFITM2, and IFITM3 Inhibit the Early Replication of Influenza A Virus

We then tested if overexpression of IFITM3, or its paralogs, IFITM1 and 2, could alter viral infection. A549 lung epithelial cells were transduced with retroviruses expressing IFITM1, 2, or 3. Two days later, the transduced cells showed increased resistance to infection with influenza A viruses PR8 (H1[PR]) or H3N2 A/Udorn/72 (H3 [Udorn], Figures 4A and 4B). Profound restriction was also seen when IFITM3 was stably overexpressed in either A549, U2OS, or primary chicken fibroblast cells (ChEFs, Figures 4C–4F and S4C). In addition, the overexpression of IFITM3 in a canine cell line used for propagating influenza A viruses (Madin-Darby canine kidney [MDCK] cells) strongly inhibited the cytopathic effect of sequential rounds of viral infection (Figures 4G and 4H) and also blocked infection by two current seasonal vaccine strains, A/Brisbane/59/07 H1N1 and A/Uruguay/716/07 H3N2, and by A/Aichi/2/68 H3N2, a viral isolate from the Hong Kong flu pandemic of 1968 (Figure S4D). This restriction was not universal because IFITM proteins did not inhibit Moloney Leukemia virus (MLV, amphotropic envelope, Figure 4A).

To address where in the life cycle the block was occurring, we used viral pseudoparticles. The pseudoparticles each contain an MLV genome encoding the enhanced green fluorescence protein (EGFP); however, each strain is uniquely coated with the envelope proteins from one of the following viruses: influenza A virus (strains H1, H3, H5, H7), Machupo virus (MACH), or MLV (Figure 4I). Overexpression of each of the IFITM proteins blocked infection by all four influenza A enveloped pseudoviruses, with

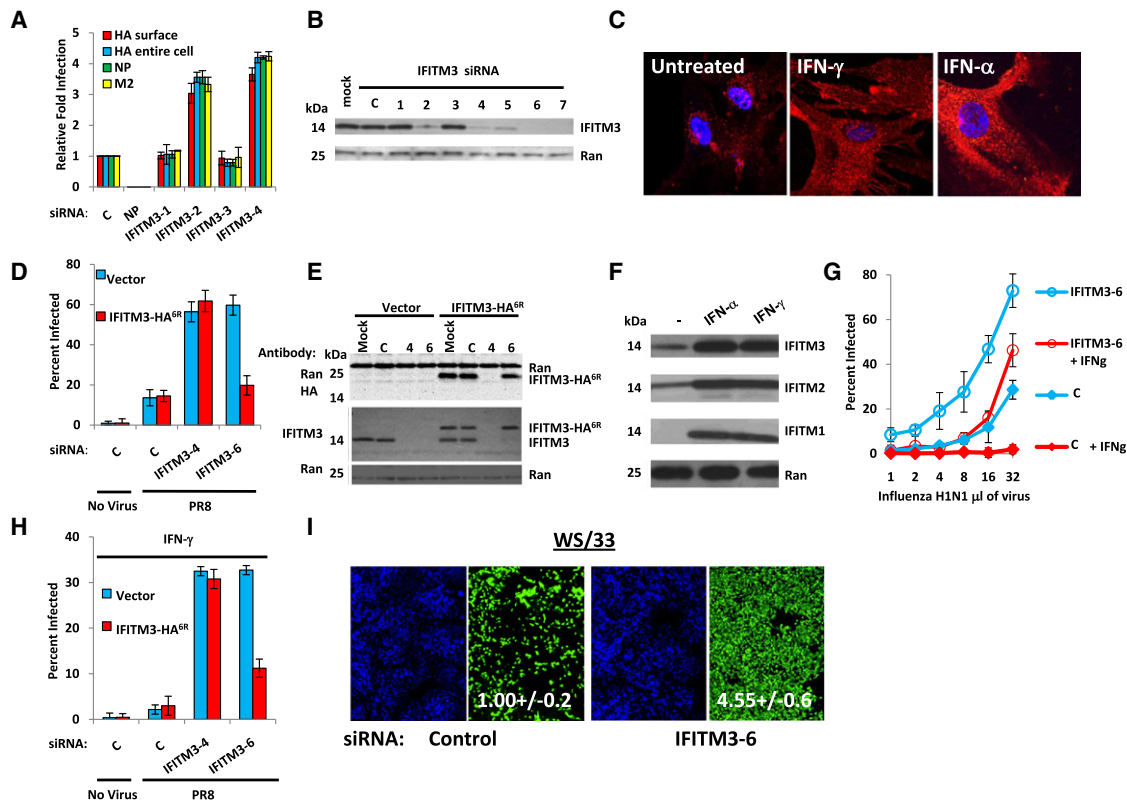


**Figure 3. IFITM3 Silencing Increases Influenza A Virus Infection and Is Required for the Antiviral Actions of Interferon**

(A) U2OS cells were transfected with the indicated siRNAs, then infected with PR8. Infection was assessed 12 hr after viral addition by IF for HA (surface or entire cell), NP, or M2. Relative fold infection is normalized to nontargeting control, C. Values represent the mean  $\pm$  SD,  $n = 3$  throughout.

(B) U2OS cells transfected with the indicated siRNAs were assessed for IFITM3 levels by western blotting.

(C) WI-38 human primary fibroblast cells stained for basal levels of IFITM3 expression (left panel) or after 24 hr treatment with IFN- $\gamma$  or IFN- $\alpha$  (red: IFITM3, blue: nuclei), 63 $\times$ .

(D) U2OS cells stably expressing either IFITM3 with a C-terminal HA-epitope tag (IFITM3-HA<sup>6R</sup>) lacking the target site for siRNA IFITM3-6 or the vector alone were transfected with the indicated siRNAs (x axis). After 72 hr the cells were incubated without (no virus) or with influenza A (PR8) for 12 hr, then stained for HA expression. The anti-HA antibody used to detect infection does not recognize the HA-epitope tag on IFITM3-HA<sup>6R</sup> (no virus, uninfected control). C, nontargeting siRNA negative control. Values represent the mean  $\pm$  SD,  $n = 3$ .

(E) U2OS cells stably expressing either IFITM3-HA<sup>6R</sup> or vector alone were transfected with the indicated siRNAs and assessed 72 hr after transfection by western blot with the indicated antibodies.

(F) U2OS cells were untreated (–) or incubated with either IFN- $\gamma$  or IFN- $\alpha$ . After 24 hr, the levels of IFITM1, 2, or 3 were checked by western blot.

(G) U2OS cells were transfected with the indicated siRNAs, then left untreated or incubated with IFN- $\gamma$  48 hr later. After 24 hr of IFN incubation, the cells were infected with increasing amounts of PR8. Twelve hours after infection the cells were stained for HA expression. Values represent the mean  $\pm$  SD,  $n = 3$ .

(H) IFITM3 is required for the antiviral effect of IFN- $\gamma$ . U2OS cells stably expressing either IFITM3-HA<sup>6R</sup> or vector were transfected with the indicated siRNAs (x axis) and treated with IFN- $\gamma$  48 hr later. After 24 hr, cells were incubated without or with influenza A (PR8), and 12 hr after infection cells were checked for HA surface expression. Values represent the mean  $\pm$  SD,  $n = 3$ .

(I) IFITM3 loss enhances infection by the H1N1 strain WS/33. U2OS cells were transfected with the indicated siRNAs for 72 hr, infected with WS/33 for 12 hr, and stained for HA expression (green, blue: nuclei). Relative fold infection is normalized to nontargeting control. Values represent the mean  $\pm$  SD,  $n = 3$ .

less restriction seen against VSV-G protein, and none against MLV ( $\gamma$ -retrovirus) or MACH (arenavirus) envelope proteins (Figures 4I, S4E, and S4F).

To complement these gain-of-function results, we depleted IFITM3 in U2OS cells, then infected with pseudoviruses expressing either influenza A virus envelope (H1[PR]) or VSV-G (Figure 4J). Decreased IFITM3 levels increased infection of the influenza A H1 pseudoviruses, with VSV-G entry elevated to a lesser extent only with the most potent siRNA, IFITM3-6 (Figure 4J). Because the life cycles of the pseudoviruses differ only in the means of entry mediated by their respective viral enve-

lopes, these data are consistent with the IFITM proteins blocking influenza A virus infection early in the viral life cycle, somewhere between and including viral-host receptor binding and entry of the vRNP into the cytosol.

Influenza A virus infection begins with the viral envelope proteins interacting with sialylated glycoproteins on the host cell's surface (Lamb and Krug, 2001). We found no reduction, and even a slight increase, in the levels of SA with IFITM proteins overexpression, pointing away from a reduction in SA underlying the actions of the IFITM proteins (Figure 4K). When the transfected cells were examined by flow cytometry, the N-terminal

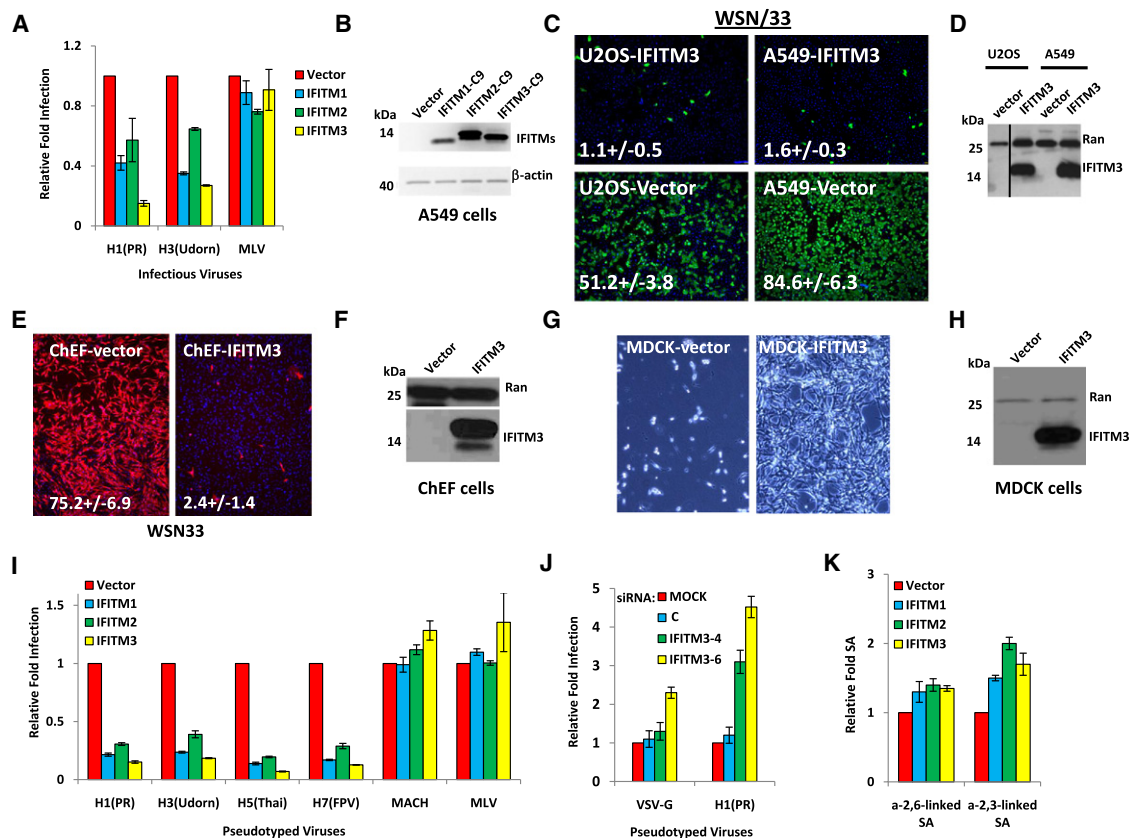


**Figure 4. The IFITM Protein Family Restricts Influenza A Virus Infection**

(A) A549 cells were transduced with retroviruses containing C9-tagged cDNAs for the indicated IFITM proteins or empty viral vector alone. After 2 days, cells were infected with one of the following viruses: PR8 (H1[PR]), influenza A virus A/Udorn/72 (H3N2) (H3[Udorn]), or Moloney murine leukemia virus (MLV). Twenty-four hours after infection, cells were checked for HA surface expression by flow cytometry. Values represent the mean  $\pm$  SD,  $n = 3$ .

(B) The expression of IFITM proteins in (A) was checked by western using anti-C9 antibody.  $\beta$ -actin levels show protein loading.

(C) A549 or U2OS cells stably overexpressing IFITM3 protein or vector alone were infected with influenza A H1N1 WSN/33. Twelve hours later, cells were fixed and stained for surface HA expression. Values represent the mean  $\pm$  SD,  $n = 3$  (green: HA, blue: nuclei; 4 $\times$ ).

(D) A549 and U2OS cells stably overexpressing IFITM3 were tested for expression by western.

(E) Primary chicken fibroblast cells (ChEFs) stably overexpressing IFITM3 protein or vector alone were infected with influenza A H1N1 WSN/33. Twelve hours later, cells were fixed and stained for surface HA expression. Values represent the mean  $\pm$  SD,  $n = 3$  (red: HA, blue: nuclei; 4 $\times$ ).

(F) ChEF cells stably overexpressing IFITM3 were tested for expression by western.

(G) MDCK cells stably overexpressing IFITM3 protein or vector alone were infected with influenza A H1N1 WSN/33 at a multiplicity of infection (moi) of 0.005. Seventy-two hours later, cells were washed with fresh media, then imaged live to assess cytopathic effect. Bright-field images shown are representative of four independent experiments (10 $\times$ ).

(H) MDCK cells stably overexpressing IFITM3 were tested for expression by western.

(I) A549 cells were transduced with retroviruses containing the indicated IFITM proteins or empty vector. Forty-eight hours later, the cells were incubated with MLV-EGFP virus pseudotyped with the indicated envelope proteins. HA proteins from various influenza A virus strains including H1 (PR): A/PR/8/34 (H1N1), H3 (Udorn): A/Udorn/72 (H3N2), H5(Thai): A/Thailand2(SP-33)/2004 (H5N1), H7(FPV): A/FPV/Rostock/34 (H7N1), MLV: MLV env protein, or MACH: Machupo virus glycoprotein. Viral entry is expressed as mean EGFP fluorescence relative to vector control cells, as measured by flow cytometry. Values represent the mean  $\pm$  SD,  $n = 3$ .

(J) U2OS cells transfected with the indicated siRNAs for 72 hr were then incubated with MLV-GFP virus pseudotyped with the VSV-G or the HA protein of PR8, H1(PR). Entry, represented as percent green fluorescing cells relative to mock-transfected cells, was determined by IF microscopy 2 days post-infection. Values represent the mean  $\pm$  SD,  $n = 4$ . C, nontargeting siRNA negative control.

(K) A549 cells were transduced with the indicated retroviruses. Forty-eight hours later, the cells were tested for surface expression of sialic acid (SA). Values represent the mean  $\pm$  SD,  $n = 3$ .

epitope tag was bound by antibody without membrane permeabilization, revealing that the N terminus is extracellular (Figure S5A). In addition, the C terminus could also be detected in IF studies using nonpermeabilized cells, demonstrating that it is also extracellular (Figure S5B, lower right panel).

#### Deletion of the Murine *Ifitm* Locus Leads to Increased Influenza A Virus Infection In Vitro

Human and murine IFITM proteins display a high degree of interspecies homology (Figure S6). Thus, to examine the evolutionary conservation of IFITM protein function, we derived murine

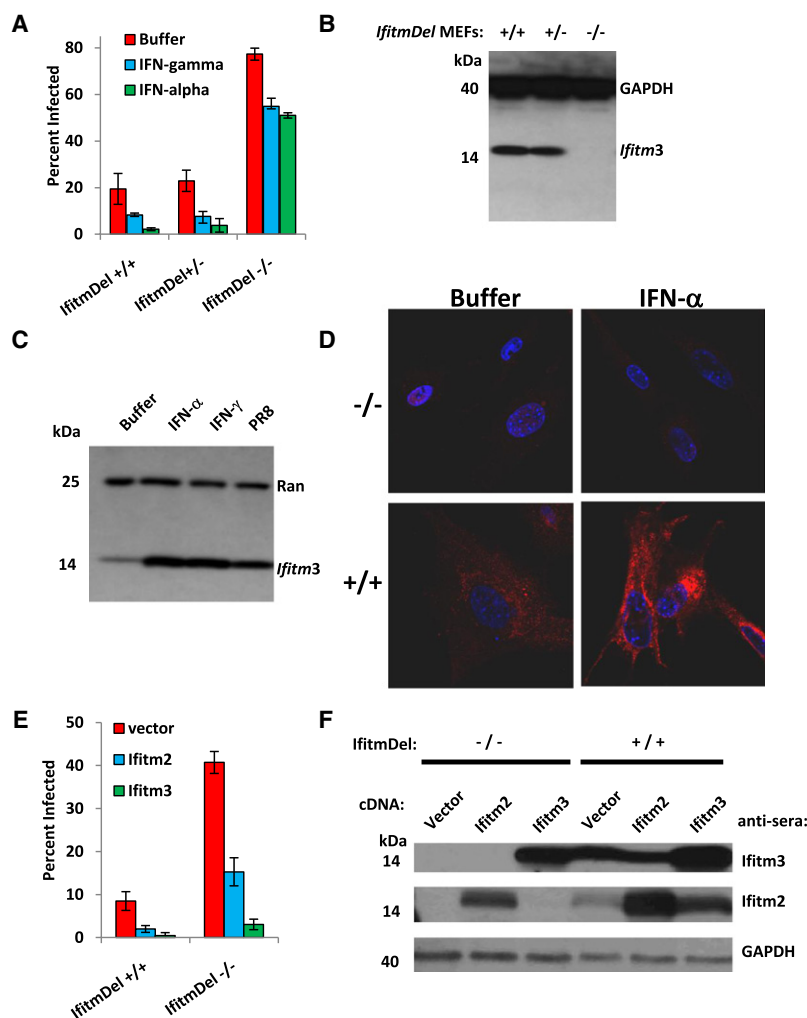


**Figure 5. *Ifitm* Knockout Cells Are More Susceptible to Influenza A H1N1 Virus Infection and Are Protected by the Reinstatement of *Ifitm2* or *3* Expression**

(A) MEFs derived from the indicated *IfitmDel* mice were left untreated (buffer) or treated with interferon- $\alpha$  or - $\gamma$ . After 24 hr, the cells were incubated with influenza A virus H1N1 (PR8). Twelve hours after infection, the cells were checked for HA surface expression. Values represent the mean  $\pm$  SD,  $n = 3$ .

(B) MEFs from (A) were assessed by western blot for the presence of Ifitm3 protein. GAPDH levels are provided to show protein loading.

(C) MEFs were left untreated (buffer) or incubated with either IFN- $\gamma$ , IFN- $\alpha$ , or PR8 virus. After 24 hr the levels of Ifitm3 were checked by western blot.

(D) *IfitmDel*<sup>+/+</sup> MEFs or *IfitmDel*<sup>-/-</sup> MEFs were incubated in the absence (buffer) or presence of IFN- $\alpha$  for 24 hr, prior to staining with  $\alpha$ -Ifitm3 (red; Ifitm3, nuclei: blue); 63 $\times$ .

(E) *IfitmDel*<sup>+/+</sup> MEFs or *IfitmDel*<sup>-/-</sup> MEFs stably expressing *Ifitm2*, *3*, or the empty vector were challenged with PR8 virus. Twelve hours later, the cells were fixed and imaged for HA expression. Values represent the mean  $\pm$  SD,  $n = 3$ . (F) The indicated MEFs were assessed for *Ifitm2* and *3* expression by western blot. GAPDH demonstrates protein loading.

embryonic fibroblasts (MEFs) from a mouse strain, *IfitmDel*, deleted for all of the *Ifitm* genes (*Ifitm1*, *2*, *3*, *5*, and *6*; Lange et al., 2008). In spite of the loss of these genes, the *IfitmDel* mice develop normally (Lange et al., 2008). Comparison of *IfitmDel*<sup>+/+</sup>, +/-, and -/- MEFs revealed a marked increase in PR8 infection in the -/- cells (Figure 5A). The differences in infection were more pronounced when the MEFs were cultured with IFN- $\alpha$  or - $\gamma$  prior to viral infection (Figures 5A–5C). As in human cells, we observed a vesicular staining pattern for Ifitm3 (Figures 5D and 3C). Forced expression of *Ifitm2* or *3* in the *IfitmDel*<sup>-/-</sup> cells restored resistance to influenza A H1N1 infection (Figures 5E and 5F). We conclude that the *Ifitm* protein family accounts for a significant proportion of the anti-influenza actions of types I and II IFNs in mice, and the majority of this function can be restored by the stable expression of *Ifitm2* or *3*.

#### IFITM3 Inhibits the Early Replication of West Nile Virus and Dengue Virus

We next explored the specificity of IFITM-mediated restriction by testing a panel of viral-like particles (VLPs) and pseudotyped viruses, each expressing a unique viral envelope protein. The

VLPs expressed the envelope proteins of one of three flaviviruses, West Nile virus (WNV), yellow fever virus (YFV), or the Omsk hemorrhagic fever virus (OMSK). These VLPs can undergo a single round of infection and are produced by transiently expressing the respective envelope proteins together with the WNV structural genes in cells stably expressing subgenomic WNV replicons containing EGFP (Yoshii and Holbrook, 2009). As observed with influenza A pseudoparticles, all three VLPs

were blocked by each of the IFITM proteins, demonstrating that these restriction factors impede first round infection (Figure 6A). Again, the IFITM proteins were found to inhibit VSV-G-mediated infection to a lesser extent (Figure 6A). In contrast, pseudoparticles expressing the envelope proteins of three arenaviruses, lymphocytic choriomeningitis virus (LCMV), Lassa virus (LASV), and MACH, or the MLV retrovirus, were not affected by IFITM expression. We next tested the effects of IFITM protein levels on two pathogenic flaviviruses, WNV and DNV. The replication of the 2741 strain of WNV was dramatically decreased in either A549 or U2OS cells stably overexpressing IFITM3 (Figures 6B and 6C). Furthermore, siRNA depletion of IFITM3 protein also led to an increase in replication of both WNV (Figures 6D and 6E) and DNV serotype 2 (New Guinea C strain, Figures 6F and 6G). However, although IFITM3 did not inhibit hepatitis C virus (HCV), a more distantly related member of the Flaviviridae family, it did block influenza A virus infection in the same HCV-permissive liver cell line (Huh 7.5.1, Figures S5D and S5E). We conclude that IFITM proteins restrict the replication of two additional human pathogens, DNV and WNV, and are likely to also limit YFV and OMSK infection based on the VLP data.

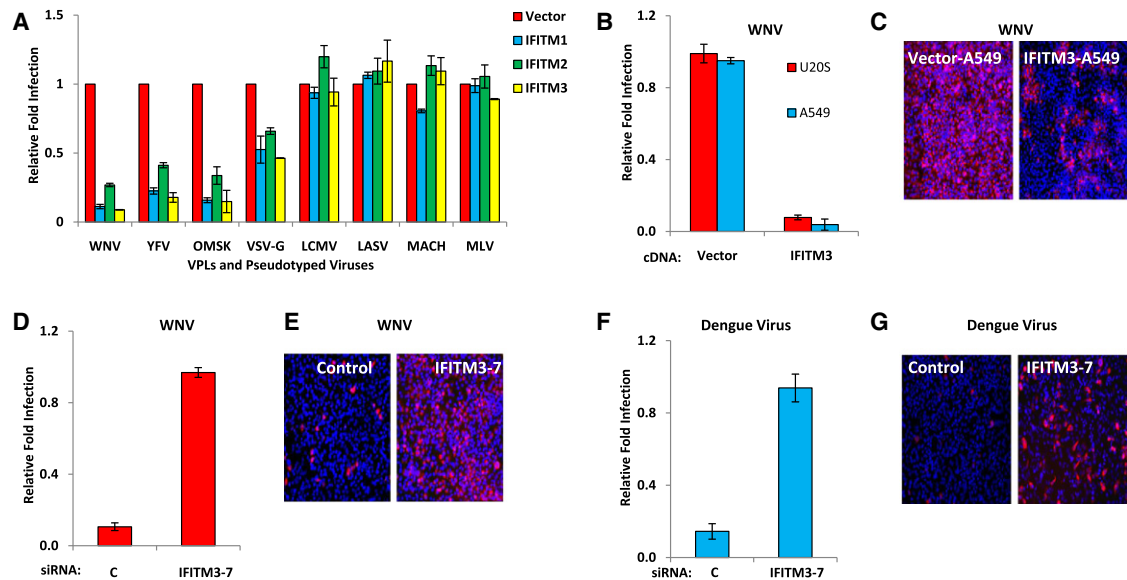


**Figure 6. The IFITM Protein Family Restricts West Nile Virus and Dengue Virus Infections**

(A) Vero E6 cells were transfected with retroviruses expressing the indicated IFITM proteins or the empty viral vector. Two days later, the cells were incubated with flaviviral viral-like particles (VLPs), expressing EGFP, and coated in envelope proteins from WNV, yellow fever virus (YFV), or Omsk virus (OMSK), or with EGFP-expressing MLV viruses pseudotyped with the indicated viral envelope proteins. Viral infection is expressed as mean EGFP fluorescence relative to vector control cells, as measured by flow cytometry 48 hr post-infection. Values represent the mean  $\pm$  SD,  $n = 3$ .

(B) A549 or U2OS cells stably expressing either IFITM3 protein or the vector alone (also shown in Figures 4C and 4D) were infected with infectious WNV (strain 2741). Twenty-four hours later, the cells were fixed and stained for viral E protein expression by IF. Values represent the mean  $\pm$  SD,  $n = 3$ .

(C) Images of A549 cells in (B) (red: WNV E protein, blue: nuclei), 4 $\times$  magnification.

(D) HeLa cells were transfected with the indicated siRNAs for 72 hr, then infected with WNV. Twenty-four hours later, the cells were fixed and stained for viral E protein. Values represent the mean  $\pm$  SD,  $n = 3$ . C, nontargeting siRNA negative control.

(E) Images of HeLa cells in (D) (red: WNV E protein, blue: nuclei), 4 $\times$  magnification.

(F) HeLa cells were transfected with the indicated siRNAs for 72 hr, then infected with dengue virus (New Guinea C strain). Thirty hours post-infection, the cells were fixed and stained for viral E protein expression by IF. Values represent the mean  $\pm$  SD,  $n = 3$ . C, non-targeting siRNA negative control.

(G) Images of HeLa cells in (F); 4 $\times$ .

## DISCUSSION

### Integrated Model of Influenza A Virus Host Factors

Although considerable knowledge exists regarding the function of viral proteins, the role of host factors in modifying infection is less understood. Therefore, we executed a genetic screen and identified over 120 human proteins needed by influenza A virus. The screen enriched for multiple host cell pathways including endosomal acidification, vesicular trafficking, mitochondrial metabolism, nucleocytoplasmic shuttling/mRNA export nuclear transport, and RNA processing.

Our findings both support and extend those of a previous screen for influenza A virus-dependency factors that used *Drosophila* cells (Hao et al., 2008). Among the factors identified in our primary screen are the human orthologs of 11 insect-cell host factors previously reported to be required for flu infection in fly cells (19.6% of the 56 identifiable human orthologs; Figure 2, Dataset S1D). Within this common set, we recovered our positive control, NXF1, as well as NUP98, EIF4A2, ARCN1, COPG, PGD, RAB5A, and RAB10. In addition to these exact candidate matches, there was strong overlap between the screens within several biologic pathways and macromolecular complexes and those of the Reactome's influenza A virus infection database

(Figure 2). This synthesis demonstrates the collective functional insights that unbiased large-scale mammalian and fly RNAi studies can provide in combination and outlines many central functions and interactions required for the flu life cycle as well as new antiviral drug targets.

We have also constructed an enrichment analysis for host factors identified in the screen (Dataset S2), including a summary comparison of enriched GO categories for three whole-genome screens for host-factor modifiers of viral infection (HIV, [Brass et al., 2008], influenza A virus [this study], and WNV [Krishnan et al., 2008]), wherein each screen's respective candidate gene list was analyzed separately for enriched GO categories. GO terms that were enriched for in one more of the screens are provided, with overlapping viral dependencies apparent for components involved in spliceosome activity, Golgi function, vesicular trafficking, and proton transport (Dataset S2). These represent a core set of functions we now know to be shared among a very diverse set of viruses.

### The IFITM Protein Family

Our screen identified the IFITM proteins as viral restriction factors. IFITM proteins were originally described 25 years ago based on their expression after IFN treatment (Friedman et al.,

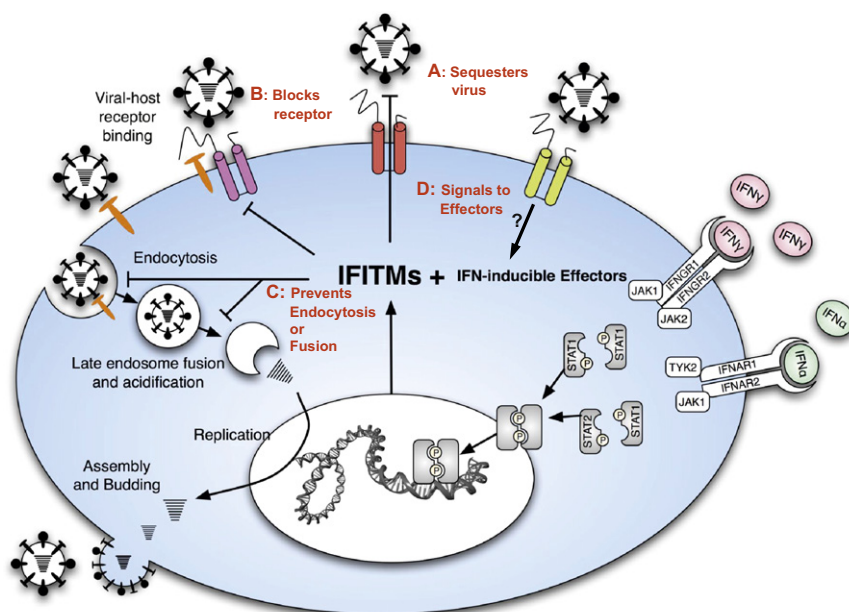


**Figure 7. IFITM Proteins Act as Antiviral Restriction Factors**

A schematic model of the influenza A virus life cycle, the induction of IFITM proteins, and their role in blocking Influenza A virus infection. IFITM1, 2, and 3 are represented by the three multitransmembrane proteins. Red lettering indicates possible mechanisms of restriction: IFITM proteins may (A) sequester the incoming viruses at or near the surface, (B) block viral receptors from interacting with host receptors (shown in orange), (C) prevent endocytosis or viral membrane fusion, (D) act as receptors and, after binding the virus, signal to effectors.

1984). The human *IFITM1*, 2, 3, and 5 genes lie adjacently on chromosome 11. *IFITM1*, 2, and 3 are nearly ubiquitously expressed whereas *IFITM5* is expressed in osteoblasts. The IFITM proteins have been ascribed roles in immune cell signaling, cell adhesion, oncogenesis, germ cell homing and maturation, and bone mineralization (Evans et al., 1993; Imai and Yoshie, 1993; Lange et al., 2003; Smith et al., 2006). However, with the exception of *IFITM5*'s role in bone mineralization, we know of no other functional studies clearly demonstrating an additional function for an IFITM family member (Moffatt et al., 2008). Indeed, in our hands, transformed and primary cells either overexpressing or depleted for *IFITM3* display no growth perturbations, and as noted, the *IfitmDel* mice develop and age normally (Lange et al., 2008).

The IFITM proteins belong to a protein domain superfamily consisting of over 30 proteins, each possessing two transmembrane domains and an intervening highly conserved intracellular loop (pfam04505, CD225, Interferon-induced transmembrane protein). Expression of members of the CD225 protein family have been reported in zebrafish, *Xenopus*, invertebrates, and bacteria, and homologs are found in frog, fish, fowl, and mammals (mouse, rat, dog, swine, cow, primate, and human; Figures S6 and S7). Now that an antiviral role has been demonstrated, it will be interesting to determine if any of the related factors participate in host-pathogen interactions and, if so, how early in evolution this protein domain became associated with innate immunity.

### The IFITM Proteins Are IFN-Inducible Restriction Factors that Inhibit Influenza A and Flaviviral Infection at Entry

A vital component of the innate immune response to viral infection is mediated by restriction factors. The antiviral action of the IFITM proteins was observed in primary human, chicken, and

mouse cells, in addition to multiple transformed cell lines, including dog cells permissive for influenza A virus replication. We also found that the IFITM proteins broadly inhibit the replication of all influenza virus strains tested, including two current vaccine strains. Furthermore, the IFITM proteins inhibit two highly pathogenic flaviviruses, WNV and DNV, and likely control YFV and OMSK, indicating a very general antiviral role. Previous work suggested that overexpression of human *IFITM1* in murine fibroblasts partially blocked infection by VSV but not by influenza A virus, although no loss-of-function experiments were reported (Alber and Staeheli, 1996). We also detected modest inhibition of VSV-G pseudoviruses but very strong inhibition of influenza A virus with all three IFITM proteins. However, the more distantly related hepatitis C virus, HCV, was not inhibited by *IFITM3* levels (Figures S5D and S5E), nor were HIV (Figure S3F) or pseudoparticles bearing the envelope proteins of multiple arenaviruses.

Basal levels of *IFITM2* and 3 were required to resist initial viral infection and so may act as first-line defenders that prevent or slow infections until the IFN system can reinforce them, by both upregulating their levels and inducing the expression of additional factors, such as *IFITM1* and *MxA* (Takaoka and Yanai, 2006). Consistent with this notion, we observed that depletion of *IFITM3* resulted in loss of 40% to 70% of IFN's protective effect, with a similar diminution also detected in the *IfitmDel* mouse cells. Thus, IFITM proteins are critical for the innate immunity to influenza A virus afforded by IFNs. These results contribute to our understanding of IFN action in that they demonstrate that these antiviral cytokines block viral entry by inducing the expression of the IFITM proteins.

### Possible Mechanisms of IFITM Restriction of Influenza and Flavivirus Infection

As schematized in Figure 7, the IFITM proteins could act at any stage of viral entry, for example by directly binding the virus and inhibiting interactions with host cell receptors (A); blocking receptor access (B); inhibiting endocytosis, preventing viral membrane fusion or rerouting vesicular traffic to a nonproductive end (C); or acting as pattern recognition receptors on the cell surface or on endocytosed vesicles where they could signal to downstream antiviral effectors (D). Logic would further predict

that IFITM proteins could target a common step in the viral life cycle. While influenza A virus and flaviviruses bind distinct receptors, both are endocytosed through a clathrin-dependent pathway, although influenza A also has a clathrin-independent pathway (Chen and Zhuang, 2008; Sieczkarski and Whittaker, 2002). After endocytosis, early endosomes containing influenza A virus fuse with late endosomes where a pH < 5.5 triggers the HA-directed fusion of the viral and endosomal membranes, permitting vRNP entry (Figure 7; Lamb and Krug, 2001). In contrast, flaviviruses undergo fusion in early endosomal compartments and at a considerably higher pH of 6.5 (Krishnan et al., 2007; Sanchez-San Martin et al., 2009). Thus, a very general overlap involving clathrin-mediated endocytosis and trafficking into early endosomes exists between influenza A virus and flaviviruses.

However, these common entry steps are shared to varying degrees by several of the viruses not impacted by IFITM proteins. For instance, sparing of the arenaviruses (MACH, LCMV, LASV) argues against a block to general endocytosis or clathrin-mediated endocytosis. Moreover, like flaviviruses, the arenaviruses also traffic in early endosomes, where they undergo pH-dependent fusion, thereby leaving no unique entry step shared by the two viral families impacted by the actions of the IFITM proteins. However, we cannot rule out that these resistant viruses may have multiple entry or endosome escape pathways or may have evolved to circumvent terminal rerouting by IFITMs. We would also note, however, that, coculture of IFITM3 overexpressing cells with parent control cells did not confer protection, suggesting a cell-autonomous mode of action (data not shown). Therefore, higher-resolution studies will now be required to determine the precise mode(s) of viral interference employed by the IFITM proteins.

We identified three additional candidate influenza A virus restriction factors: PUSL1, TPST1, and WDR33. It is possible that these might work together with IFITM proteins to execute viral resistance, and it remains to be determined whether they block at the same point in the life cycle. WDR33 is an orphan WD40 repeat protein about which little is known. TPST1 is a Golgi-localized transmembrane tyrosylprotein sulfotransferase that is known to sulfonate proteins destined for the cell surface or secretion (Hoffhines et al., 2006). PUSL1 shares homology with pseudouridylylase genes that modify RNA by converting uridine into pseudouridine, a glycosylated form of uracil, in several cytosolic and mitochondrial transfer RNAs (tRNAs) (Massenet et al., 1999). While further validation is warranted, it is tempting to speculate that PUSL1 could potentially block influenza by directly modifying viral RNA.

The IFITM proteins and other innate cell-intrinsic defenders present opportunities not just for a greater understanding of fundamental questions but also as tools to actively combat current and emerging pathogens. Variations in the basal and inducible levels of these factors as well as the dependency factors within a population might predict the severity of flu or flaviviral infections among individuals or across species. The discovery of the roles of IFITM proteins in innate immunity has relevance to ongoing and future influenza pandemics. Not only could elucidation of the IFITM restriction mechanism prove important in designing new antiviral therapies, but the proteins

themselves could be used in multiple ways to fight influenza A, WNV, and dengue virus. If IFITM proteins work on the plasma membrane, they could possibly be delivered to tissues susceptible to initial infection by liposomal transfer. Transgenic animals such as fowl or swine could be developed that overexpress IFITM proteins to provide resistance to influenza A virus and other pathogens, thereby preventing the spread of these viruses, as well as limiting their ability to recombine with human influenza A strains to produce strains dangerous to human populations. Indeed, by creating animals with multiple transgenic restriction factors, we can confront the virus with a more intractable barrier. Finally, if IFITM proteins are also rate limiting for influenza A virus infection in other organisms such as chickens, whose embryos are employed to passage attenuated viruses for vaccine production, the inhibition of IFITM protein expression could reduce the amount of time it takes to produce vaccine and thereby boost yields. This has been a critical issue confounding vaccine production in the current influenza pandemic. The discovery of the role of IFITM proteins as antiviral agents for multiple devastating pathogenic viruses has given us new insights into innate immunity and has provided us new tools with which to counter viral propagation in the future.

## EXPERIMENTAL PROCEDURES

### siRNA Screen

For the siRNA screen we employed an arrayed library targeting 17,877 genes (Dharmacon siARRAY siRNA Library; Human Genome, G-005000-05, Thermo Fisher Scientific, Lafayette, CO). siRNAs were transiently reverse transfected into the U2OS cells in triplicate at a 50 nM final concentration, using a final concentration of 0.32% Oligofectamine (Invitrogen) in a 384-well format. After 72 hr, the medium was removed and the cells were infected with the Influenza A/Puerto Rico/8/34 (PR8, ATCC VR-1469), multiplicity of infection (moi) of ~0.2–0.3 in 40  $\mu$ l complete media. After 12 hr, media were removed, and cells were fixed with 4% formalin and stained with anti-HA antibodies (Hybridoma HA36-4-5.2, Wistar Institute), followed by an Alexa Fluor 488 goat anti-mouse secondary at 1:1,000 (A11001, Invitrogen). Cells were imaged on an automated Image Express Micro (IXM) microscope (Molecular Devices) and analyzed using the Metamorph Cell Scoring software program (Molecular Devices Inc.). The validation round for single siRNAs was done as described previously (Brass et al., 2008). All Dharmacon siRNAs and plasmids used for generating stable cell lines are shown in Dataset S1 and the Supplemental Experimental Procedures.

### Cell Lines and Culture Conditions

U2OS, A549, MDCK, 293T, Huh7.5.1, primary Chicken fibroblast cells (ChEFs, Charles River Labs), Vero E6, and HeLa cells were grown in DMEM (Invitrogen Cat#11965) with 10% FBS (Invitrogen). WI-38 cells were cultured in DMEM (Invitrogen Cat#10569), containing 1  $\times$  MEM nonessential amino acids (Invitrogen Cat#11140, 10 mM stock/100 $\times$ ) and 15% FBS. Adult *IfitmDel<sup>+/−</sup>* mice (Lange et al., 2008) were intercrossed and fibroblasts (MEFs) derived from embryos at day 13.5 of gestation, as described previously (Nagy et al., 2003) and in the Supplemental Experimental Procedures.

### Viral Propagation and Titration

Influenza A (H1N1) A/PR/8/34 (ATCC VR-1469), influenza A (H1N1) A/WS/33 (ATCC VR-1520), influenza A (H1N1) A/WSN/33, and influenza (H3N2) A/Udm/72 were propagated and viral infectivity was titrated as previously described (Huang et al., 2008). Hybrid Moloney/Amphotropic murine leukemia virus (MLV, ATCC VR-1450) was propagated in NIH 3T3 cells. WNV (strain 2741) and DNV serotype 2 (New Guinea C strain) viruses were grown on Vero cells.

### West Nile and Dengue Virus Infections

West Nile (strain 2741) and dengue serotype 2 (New Guinea C strain) viruses were used to infect the IFITM3-silenced HeLa cells at an moi of 0.1 for 24 or 30 hr, respectively, as reported previously (Krishnan et al., 2008). Infected cells were fixed in 4% PFA and immunostained with antibodies detecting viral E-proteins (Chemicon) and imaged by fluorescence microscopy (Zeiss). IFITM3 overexpressing or vector control-A549 or -U2OS cells were infected with WNV at an moi of 1.

### Influenza A Virus and MLV Infection

Influenza A virus A/PR/8/34 (H1N1) (moi = 5), A/Udm/72 (H3N2) (moi = 1), and MLV were used to infect A549 cells expressing different IFITM proteins. Twenty-four hours later, infected cells were labeled with murine anti-influenza viral H1 IgG<sub>2a</sub> (C179), anti-influenza viral H3 IgG<sub>1</sub> (F49) (Takara Bio. Cat#M145 and M146), or goat anti-MLV env polyclonal antibodies (ATCC) and stained with PE-conjugated anti-mouse or anti-goat secondary antibodies. Cells were then fixed with 1% formaldehyde and analyzed by flow cytometry.

### Viral-like Particles and Pseudotyped Virus

MLV-GFP pseudoviruses were made as described (Huang et al., 2006, 2008). Flavivirus VLP were as described (Hanna et al., 2005), except plasmids encoding structure proteins of WNV (strain NY99), yellow fever virus (strain D17), or Omsk hemorrhagic fever virus (Ref. Seq.: NP\_878909.1) were used. VLP and pseudovirus entry in A549 or Vero E6 cells expressing IFITM proteins was assessed 2 days later by measuring GFP expression by flow cytometry. The infection level of siRNA-transfected U2OS cells after 2 days of infection was determined by calculating the percent of GFP-positive cells by IF after fixation with 4% PFA and staining of nuclei with Hoechst 33342.

Intracellular HA-staining was performed as above with the exception that after PFA fixation, cells were incubated in 0.1%–0.2% Tween 20 (Sigma), then blocked in 1% BSA with 0.3M glycine in D-PBS, prior to staining with the primary antibody. This identical protocol was used with staining for NP (Abcam, AA5H, ab20343, 1:1000), M2 (Abcam, 14C2, ab5416, 1:1000), Anti-HA7 from Sigma-Aldrich (Product code H 3663), which recognizes the HA non-peptide tag on IFITM3<sup>RP</sup> but not PR8's HA, and monoclonal antibody against human influenza A virus (H1N1, H2N2) (Takara, C179, Cat#M145, 1:1000), which recognizes the HA of WS/33 but not of PR8. Sialic acid staining has been described (Huang et al., 2006, 2008).

### Enrichment Analysis

Statistical analysis of gene enrichment was performed using a hypergeometric distribution as described in the GOHyperGAll module of Bioconductor for gene ontology terms (Gentleman et al., 2004). A map of the viral life cycle was created by connected keywords. Genes were mapped to these keywords using a database that integrates annotation information from UniProt (Bairoch et al., 2005), KEGG (Kanehisa et al., 2004), Reactome (Vastrik et al., 2007), Gene Ontology (Ashburner et al., 2000), and NCBI GeneRIF (Mitchell et al., 2003); in addition, OMIM Human orthologs were mapped to other species using NCBI HomoloGene (Wheeler et al., 2005) (see Supplemental Experimental Procedures for more details).

Additional Experimental Procedures are included in the Supplemental Data.

### SUPPLEMENTAL DATA

Supplemental Data include Supplemental Discussion, Supplemental Experimental Procedures, seven figures, and two datasets and can be found with this article online at [http://www.cell.com/supplemental/S0092-8674\(09\)01564-5](http://www.cell.com/supplemental/S0092-8674(09)01564-5).

### ACKNOWLEDGMENTS

We thank the ICCB-Longwood; C. Shamu, S. Chang, S. Rudnicki, S. Johnston, K. Rudnicki, D. Wrobel, M. Ocana, and Z. Cooper; Ragon Institute; L. White-man, K. Hartman, A. Piechocka-Trocha, J. Proudfoot, and T. Diefenbach. We thank J. Philips, A. Mehle, M. Franti, F. Diaz-Griffero, J. Mabry (CDC), and J. Chou for helpful discussions. Funding support: A.L.B. wishes to express

his gratitude to the Phillip T. and Susan M. Ragon Foundation for their generous support. A.L.B. (MGH GI Unit, Harvard Center for AIDS Research); M.N.K. and E.F. (NIH grants AI 50031 and AI070343); Y.B. and R.J.X. (CSIBD, CCIB, Genetics and Genomics Core, and NIH grants AI062773, DK060049, and DK043351); I.C.H. and M.F. (NERCE U54 AI057159). D.J.A. is supported by Cancer Research UK and the Wellcome Trust. L.v.d.W. is supported by a fellowship from the Kay Kendall Leukaemia Foundation. This study was supported by the New England Regional Center of Excellence for Biodefense and Emerging Infectious Diseases (NIH grant U54 AI057159 to D. Kasper). S.J.E. and E.F. are Investigators with the Howard Hughes Medical Institute.

Received: November 5, 2009

Revised: December 1, 2009

Accepted: December 9, 2009

Published online: December 17, 2009

### REFERENCES

- Alber, D., and Staeheli, P. (1996). Partial inhibition of vesicular stomatitis virus by the interferon-induced human 9-27 protein. *J. Interferon Cytokine Res.* 16, 375–380.
- Ashburner, M., Ball, C.A., Blake, J.A., Botstein, D., Butler, H., Cherry, J.M., Davis, A.P., Dolinski, K., Dwight, S.S., Eppig, J.T., et al. (2000). Gene ontology: tool for the unification of biology. The Gene Ontology Consortium. *Nat. Genet.* 25, 25–29.
- Bairoch, A., Apweiler, R., Wu, C.H., Barker, W.C., Boeckmann, B., Ferro, S., Gasteiger, E., Huang, H., Lopez, R., Magrane, M., et al. (2005). The Universal Protein Resource (UniProt). *Nucleic Acids Res.* 33, D154–D159.
- Boulo, S., Akarsu, H., Ruigrok, R.W., and Baudin, F. (2007). Nuclear traffic of influenza virus proteins and ribonucleoprotein complexes. *Virus Res.* 124, 12–21.
- Bouloy, M., Plotch, S.J., and Krug, R.M. (1978). Globin mRNAs are primers for the transcription of influenza viral RNA in vitro. *Proc. Natl. Acad. Sci. USA* 75, 4886–4890.
- Brass, A.L., Dykxhoorn, D.M., Benita, Y., Yan, N., Engelman, A., Xavier, R.J., Lieberman, J., and Elledge, S.J. (2008). Identification of host proteins required for HIV infection through a functional genomic screen. *Science* 319, 921–926.
- Cai, H., Reinisch, K., and Ferro-Novick, S. (2007). Coats, tethers, Rab, and SNAREs work together to mediate the intracellular destination of a transport vesicle. *Dev. Cell* 12, 671–682.
- Chen, C., and Zhuang, X. (2008). Epsin 1 is a cargo-specific adaptor for the clathrin-mediated endocytosis of the influenza virus. *Proc. Natl. Acad. Sci. USA* 105, 11790–11795.
- Evans, S.S., Collea, R.P., Leasure, J.A., and Lee, D.B. (1993). IFN- $\alpha$  induces homotypic adhesion and Leu-13 expression in human B lymphoid cells. *J. Immunol.* 150, 736–747.
- Friedman, R.L., Manly, S.P., McMahon, M., Kerr, I.M., and Stark, G.R. (1984). Transcriptional and posttranscriptional regulation of interferon-induced gene expression in human cells. *Cell* 38, 745–755.
- Ge, Q., McManus, M.T., Nguyen, T., Shen, C.H., Sharp, P.A., Eisen, H.N., and Chen, J. (2003). RNA interference of influenza virus production by directly targeting mRNA for degradation and indirectly inhibiting all viral RNA transcription. *Proc. Natl. Acad. Sci. USA* 100, 2718–2723.
- Gentleman, R.C., Carey, V.J., Bates, D.M., Bolstad, B., Dettling, M., Dudoit, S., Ellis, B., Gautier, L., Ge, Y., Gentry, J., et al. (2004). Bioconductor: open software development for computational biology and bioinformatics. *Genome Biol.* 5, R80.
- Glodowski, D.R., Chen, C.C., Schaefer, H., Grant, B.D., and Rongo, C. (2007). RAB-10 regulates glutamate receptor recycling in a cholesterol-dependent endocytosis pathway. *Mol. Biol. Cell* 18, 4387–4396.
- Hale, B.G., Randall, R.E., Ortin, J., and Jackson, D. (2008). The multifunctional NS1 protein of influenza A viruses. *J. Gen. Virol.* 89, 2359–2376.
- Haller, O., Staeheli, P., and Kochs, G. (2009). Protective role of interferon-induced Mx GTPases against influenza viruses. *Rev. Sci. Tech.* 28, 219–231.

- Hanna, S.L., Pierson, T.C., Sanchez, M.D., Ahmed, A.A., Murtadha, M.M., and Doms, R.W. (2005). N-linked glycosylation of west nile virus envelope proteins influences particle assembly and infectivity. *J. Virol.* *79*, 13262–13274.
- Hao, L., Sakurai, A., Watanabe, T., Sorensen, E., Nidom, C.A., Newton, M.A., Ahlquist, P., and Kawaoka, Y. (2008). Drosophila RNAi screen identifies host genes important for influenza virus replication. *Nature* *454*, 890–893.
- Hoffhines, A.J., Damoc, E., Bridges, K.G., Leary, J.A., and Moore, K.L. (2006). Detection and purification of tyrosine-sulfated proteins using a novel anti-sulfotyrosine monoclonal antibody. *J. Biol. Chem.* *281*, 37877–37887.
- Huang, I.C., Bosch, B.J., Li, F., Li, W., Lee, K.H., Ghiran, S., Vasilieva, N., Dermody, T.S., Harrison, S.C., Dormitzer, P.R., et al. (2006). SARS coronavirus, but not human coronavirus NL63, utilizes cathepsin L to infect ACE2-expressing cells. *J. Biol. Chem.* *281*, 3198–3203.
- Huang, I.C., Li, W., Sui, J., Marasco, W., Choe, H., and Farzan, M. (2008). Influenza A virus neuraminidase limits viral superinfection. *J. Virol.* *82*, 4834–4843.
- Imai, T., and Yoshie, O. (1993). C33 antigen and M38 antigen recognized by monoclonal antibodies inhibitory to syncytium formation by human T cell leukemia virus type 1 are both members of the transmembrane 4 superfamily and associate with each other and with CD4 or CD8 in T cells. *J. Immunol.* *151*, 6470–6481.
- Kanehisa, M., Goto, S., Kawashima, S., Okuno, Y., and Hattori, M. (2004). The KEGG resource for deciphering the genome. *Nucleic Acids Res.* *32*, D277–D280.
- Krishnan, M.N., Sukumaran, B., Pal, U., Agaisse, H., Murray, J.L., Hodge, T.W., and Fikrig, E. (2007). Rab 5 is required for the cellular entry of dengue and West Nile viruses. *J. Virol.* *81*, 4881–4885.
- Krishnan, M.N., Ng, A., Sukumaran, B., Gilfoy, F.D., Uchil, P.D., Sultana, H., Brass, A.L., Adamez, R., Tsui, M., Qian, F., et al. (2008). RNA interference screen for human genes associated with West Nile virus infection. *Nature* *455*, 242–245.
- Lamb, R.A., and Krug, R.M. (2001). Orthomyxoviridae: The viruses and their replication, Fourth Edition (Philadelphia: Lippincott Williams and Wilkins).
- Lange, U.C., Saitou, M., Western, P.S., Barton, S.C., and Surani, M.A. (2003). The fragilis interferon-inducible gene family of transmembrane proteins is associated with germ cell specification in mice. *BMC Dev. Biol.* *3*, 1.
- Lange, U.C., Adams, D.J., Lee, C., Barton, S., Schneider, R., Bradley, A., and Surani, M.A. (2008). Normal germ line establishment in mice carrying a deletion of the Ifitm/Fragilis gene family cluster. *Mol. Cell. Biol.* *28*, 4688–4696.
- Lewin, A.R., Reid, L.E., McMahon, M., Stark, G.R., and Kerr, I.M. (1991). Molecular analysis of a human interferon-inducible gene family. *Eur. J. Biochem.* *199*, 417–423.
- Maines, T.R., Szretter, K.J., Perrone, L., Belsler, J.A., Bright, R.A., Zeng, H., Tumpey, T.M., and Katz, J.M. (2008). Pathogenesis of emerging avian influenza viruses in mammals and the host innate immune response. *Immunol. Rev.* *225*, 68–84.
- Massenet, S., Motorin, Y., Lafontaine, D.L., Hurt, E.C., Grosjean, H., and Branlant, C. (1999). Pseudouridine mapping in the *Saccharomyces cerevisiae* spliceosomal U small nuclear RNAs (snRNAs) reveals that pseudouridine synthase pus1p exhibits a dual substrate specificity for U2 snRNA and tRNA. *Mol. Cell. Biol.* *19*, 2142–2154.
- Mitchell, J.A., Aronson, A.R., Mork, J.G., Folk, L.C., Humphrey, S.M., and Ward, J.M. (2003). Gene indexing: characterization and analysis of NLM's GeneRIFs. *AMIA Annu. Symp. Proc.* *2003*, 460–464.
- Moffatt, P., Gaumond, M.H., Salois, P., Sellin, K., Bessette, M.C., Godin, E., de Oliveira, P.T., Atkins, G.J., Nanci, A., and Thomas, G. (2008). Bril: a novel bone-specific modulator of mineralization. *J. Bone Miner. Res.* *23*, 1497–1508.
- Monto, A.S. (2009). The risk of seasonal and pandemic influenza: prospects for control. *Clin. Infect. Dis.* *48* (Suppl 1), S20–S25.
- Morriswood, B., Ryzhakov, G., Puri, C., Arden, S.D., Roberts, R., Dendrou, C., Kendrick-Jones, J., and Buss, F. (2007). T6BP and NDP52 are myosin VI binding partners with potential roles in cytokine signalling and cell adhesion. *J. Cell Sci.* *120*, 2574–2585.
- Nagy, A., Gertsenstein, M., Vintersten, K., and Behringer, R. (2003). Manipulating the mouse embryo (Cold Spring Harbor, NY: Cold Spring Harbor Laboratory Press).
- Nakhaei, P., Genin, P., Civas, A., and Hiscott, J. (2009). RIG-I-like receptors: sensing and responding to RNA virus infection. *Semin. Immunol.* *21*, 215–222.
- Sanchez-San Martin, C., Liu, C.Y., and Kielian, M. (2009). Dealing with low pH: entry and exit of alphaviruses and flaviviruses. *Trends Microbiol.* *17*, 514–521.
- Sieczkarski, S.B., and Whittaker, G.R. (2002). Influenza virus can enter and infect cells in the absence of clathrin-mediated endocytosis. *J. Virol.* *76*, 10455–10464.
- Sieczkarski, S.B., and Whittaker, G.R. (2003). Differential requirements of Rab5 and Rab7 for endocytosis of influenza and other enveloped viruses. *Traffic* *4*, 333–343.
- Skehel, J.J., and Wiley, D.C. (1995). Influenza viruses and cell membranes. *Am. J. Respir. Crit. Care Med.* *152*, S13–S15.
- Smith, R.A., Young, J., Weis, J.J., and Weis, J.H. (2006). Expression of the mouse fragilis gene products in immune cells and association with receptor signaling complexes. *Genes Immun.* *7*, 113–121.
- Stevens, S.W., Barta, I., Ge, H.Y., Moore, R.E., Young, M.K., Lee, T.D., and Abelson, J. (2001). Biochemical and genetic analyses of the U5, U6, and U4/U6 x U5 small nuclear ribonucleoproteins from *Saccharomyces cerevisiae*. *RNA* *7*, 1543–1553.
- Takaoka, A., and Yanai, H. (2006). Interferon signalling network in innate defence. *Cell. Microbiol.* *8*, 907–922.
- Vastrik, I., D'Eustachio, P., Schmidt, E., Gopinath, G., Croft, D., de Bono, B., Gillespie, M., Jassal, B., Lewis, S., Matthews, L., et al. (2007). Reactome: a knowledge base of biologic pathways and processes. *Genome Biol.* *8*, R39.
- Wheeler, D.L., Barrett, T., Benson, D.A., Bryant, S.H., Canese, K., Church, D.M., DiCuccio, M., Edgar, R., Federhen, S., Helmberg, W., et al. (2005). Database resources of the National Center for Biotechnology Information. *Nucleic Acids Res.* *33*, D39–D45.
- Yoshii, K., and Holbrook, M.R. (2009). Sub-genomic replicon and virus-like particles of Omsk hemorrhagic fever virus. *Arch. Virol.* *154*, 573–580.

# WDR5 is essential for assembly of the VISA-associated signaling complex and virus-triggered IRF3 and NF- $\kappa$ B activation

Yan-Yi Wang, Li-Juan Liu, Bo Zhong, Tian-Tian Liu, Ying Li, Yan Yang, Yong Ran, Shu Li, Po Tien, and Hong-Bing Shu<sup>1</sup>

College of Life Sciences, Modern Virology Center, Wuhan University, Wuhan 430072, China

Edited by Philippa Marrack, Howard Hughes Medical Institute/National Jewish, Denver, CO, and approved November 20, 2009 (received for review August 7, 2009)

**Viral infection causes activation of the transcription factors NF- $\kappa$ B and IRF3, which collaborate to induce type I interferons (IFNs) and cellular antiviral response. The mitochondrial outer membrane protein VISA acts as a critical adapter for assembling a virus-induced complex that signals NF- $\kappa$ B and IRF3 activation. Using a biochemical purification approach, we identified the WD repeat protein WDR5 as a VISA-associated protein. WDR5 was recruited to VISA in a viral infection dependent manner. Viral infection also caused translocation of WDR5 from the nucleus to mitochondria. Knockdown of WDR5 impaired the formation of virus-induced VISA-associated complex. Consistently, knockdown of WDR5 inhibited virus-triggered activation of IRF3 and NF- $\kappa$ B as well as transcription of the *IFNB1* gene. These findings suggest that WDR5 is essential in assembling a virus-induced VISA-associated complex and plays an important role in virus-triggered induction of type I IFNs.**

innate immunity | interferon | mitochondrial signal transduction

**V**iral infections are sensed by pattern-recognition receptors (PRRs) of the innate immune system that recognize pathogen-associated molecular patterns (PAMPs). Viral RNAs as PAMPs are recognized by membrane-bound toll-like receptors (TLRs), such as TLR3, 7, and 8, as well as the cytosolic RIG-I-like receptor (RLR) family members RIG-I, MDA5, and Lgp2 (1–4). Recognition of viral RNAs by the PRRs triggers a series of signaling events that lead to induction of type I interferons (IFNs). Type I IFNs activate the JAK-STAT signal transduction pathways, leading to transcriptional induction of a wide range of downstream antiviral genes and subsequent innate antiviral response (5–8).

Transcriptional induction of type I IFN genes requires the coordinate activation of multiple transcription factors and their cooperative assembly into transcriptional enhancer complexes *in vivo*. For example, the *IFNB1* gene promoter contains conserved enhancer elements recognized by NF- $\kappa$ B ( $\kappa$ B site) and phosphorylated IRF3 (ISRE site, also known as PRDIII or IRF-E). It has been shown that transcriptional activation of the *IFNB1* gene requires coordinate and cooperative assembly of an enhancosome that contains all of these transcription factors (7, 9).

In the past several years, considerable progress has been achieved on the molecular mechanisms of RLR-mediated induction of type I IFNs. Both RIG-I and MDA5 contain two CARD modules at their N terminus and a DexD/H-box RNA helicase domain at their C terminus (10, 11). Upon viral infection, the RNA helicase domains of RIG-I and MDA5 serve as intracellular viral RNA receptors, whereas their CARD modules are associated with the downstream CARD-containing adapter protein VISA (also known as MAVS, IPS-1, and Cardif) (12–16). VISA-deficient mouse embryonic fibroblasts and conventional dendritic cells (DCs) are defective in producing type I IFNs and proinflammatory cytokines in response to viruses and VISA-deficient mice were susceptible to infection with various viruses, suggesting an essential role for VISA in virus-triggered innate antiviral response (12, 17). The C terminus of VISA contains a transmembrane domain that anchors VISA to the outer membrane of mitochondria, implying an important role of mitochondria in innate antiviral immunity (15). The importance

of VISA in innate antiviral response is also illustrated by the observation that HCV encoded NS3/4A protease cleaves VISA off the mitochondria, resulting in abrogation of type I IFN induction and chronic HCV infection (14).

On the outer membrane of mitochondria, VISA acts as a central adapter for assembling a virus-induced complex that activates distinct signaling pathways leading to IRF3 and NF- $\kappa$ B activation. VISA is constitutively associated with another mitochondrion-associated adapter protein MITA/STING, which is also essential for virus-triggered signaling (18–20). It has also been reported that VISA is associated with NLRX1, a nucleotide-binding domain and leucine-rich-repeat containing family member, which functions as a brake to regulate virus-triggered signaling (21). VISA is associated with TRAF2 and TRAF6 through its TRAF interaction motifs (16). It has been shown that TRAF2 and TRAF6 facilitate K63-linked polyubiquitination of RIP and NEMO respectively. These processes lead to activation of IKK and subsequent NF- $\kappa$ B (22). VISA is also associated with TRAF3, another member of the TRAF protein family. Gene knockout studies have demonstrated that TRAF3 is essential in virus-triggered IRF3 activation (23–25).

In this report, we identified WDR5 as a component of the VISA-associated complex. Viral infection caused translocation of WDR5 to the mitochondria and association with VISA. Knockdown of WDR5 by RNAi impaired formation of virus-induced VISA-associated complex and inhibited virus-triggered NF- $\kappa$ B and IRF3 activation. Our findings suggest that WDR5 is essential for virus-induced assembly of the VISA-associated complex and induction of type I IFNs.

## Results

**Identification of WDR5 as a VISA-Associated Protein.** VISA plays a central role in assembling a complex mediating virus-triggered IRF3 and NF- $\kappa$ B activation. To identify potential new components associated with VISA, we performed Tandem Affinity Purification (TAP) experiments with VISA as a bait protein. An expression plasmid for VISA tagged with Calmodulin Binding Peptide (CBP) and Streptavidin Binding Peptide (SBP) was stably transfected into 293 cells, and VISA-associated proteins were purified by a TAP purification system. The eluted proteins were identified by a shot-gun mass spectrum analysis method. By comparing with other nonrelated purifications using the same method, we identified WDR5 as a protein specifically associated with VISA (Fig. S1). WDR5 is a WD repeat protein that has been shown to be a com-

Author contributions: Y.-Y.W., P.T., and H.-B.S. designed research; Y.-Y.W., L.-J.L., B.Z., T.-T.L., Y.L., Y.Y., Y.R., and S.L. performed research; Y.-Y.W., P.T., and H.-B.S. analyzed data; and Y.-Y.W. and H.-B.S. wrote the paper.

The authors declare no conflict of interest.

This article is a PNAS Direct Submission.

<sup>1</sup>To whom correspondence should be addressed: E-mail: shuh@whu.edu.cn.

This article contains supporting information online at [www.pnas.org/cgi/content/full/0908967107/DCSupplemental](http://www.pnas.org/cgi/content/full/0908967107/DCSupplemental).

ponent of the mixed lineage leukemia (MLL) complex, which methylates lysine 4 of histone H3 (26–28). It has also been demonstrated that WDR5 is developmentally expressed in osteoblasts and required for osteoblast differentiation (29, 30). EST profile analysis using the GenBank databases indicated that WDR5 was ubiquitously expressed in most tissues, suggesting a broader role for WDR5 in addition to osteoblast differentiation.

To determine whether WDR5 indeed interacts with VISA, we performed transient transfection and coimmunoprecipitation experiments. The results indicated that WDR5 could interact with VISA (Fig. 1A). In the same experiments, WDR5 also interacted with TRAF3 and TRAF6 but not RIG-I, MITA, TBK1, or IRF3 (Fig. 1A). Interestingly, the C terminus of VISA, which contains its transmembrane domain, was required and sufficient for its interaction with WDR5 (Fig. 1B). Previous studies suggest a nuclear function for WDR5 as a component of the MLL complex, and it is unknown whether WDR5 has a role in the cytoplasm. We isolated nuclear and cytoplasmic fractions and found surprisingly that WDR5 was more abundantly localized in the cytoplasm than in the nucleus (Fig. S2). Endogenous coimmunoprecipitation experiments indicated that WDR5 barely interacted with VISA under physiological conditions, but their interaction was markedly increased at 2 and 6 h after Sendai virus (SeV) infection (Fig. 1C). In similar experiments, the association of WDR5 with TRAF3 was also increased at 2 and 6 h after SeV infection whereas WDR5 constitutively interacted with TRAF6 (Fig. 1C). The associations of WDR5 with VISA, TRAF3, and TRAF6 were diminished at 12 h after viral infection (Fig. 1C). These results suggest that viral infection promotes the association of WDR5 with VISA or TRAF3, whereas WDR5 constitutively interacts with TRAF6.

### Viral Infection Causes Translocation of WDR5 to the Mitochondria.

Previously, it has been demonstrated that VISA is localized to the outer membrane of mitochondria (15). Because WDR5 is associated with VISA following viral infection, we determined whether WDR5 is translocated to the mitochondria following viral infection. We performed cellular fractionation experiments and found that in the absence of viral infection, WDR5 was mostly localized in the cytosol and only trace amount of WDR5 was detected in the mitochondrial fraction. However, after SeV infection, mitochondrion-associated WDR5 was markedly increased, whereas the cytosolic and whole cell WDR5 levels were not markedly changed after viral infection (Fig. 2A). Confocal microscopy and cellular fractionation experiments further indicated that viral infection caused marked translocation of WDR5 to the mitochondria, which was probably originated from the nucleus because viral infection caused decrease of WDR5 in the nucleus (Fig. 2B and C). These results suggest that viral infection caused recruitment of WDR5 to the mitochondria.

### WDR5 Is Required for Virus-Triggered Activation of IRF3 and NF- $\kappa$ B and Transcription of the *IFNB1* Gene.

Because WDR5 is translocated to the mitochondria and associated with VISA after viral infection, we determined whether WDR5 is involved in virus-triggered type I IFN signaling. We made four WDR5 RNAi constructs and determined their effects on knockdown of WDR5. As shown in Fig. 3A, the #3 WDR5-RNAi construct could inhibit expression of transfected WDR5 to 10% of the control sample ( $P < 0.01$ ). The #1 and #4 RNAi constructs could reduce WDR5 levels to 70% and 60% of the control sample, respectively, whereas the #2 RNAi plasmid had no effect. The #3 WDR5-RNAi construct also markedly inhibited expression of endogenous WDR5 protein either without or with

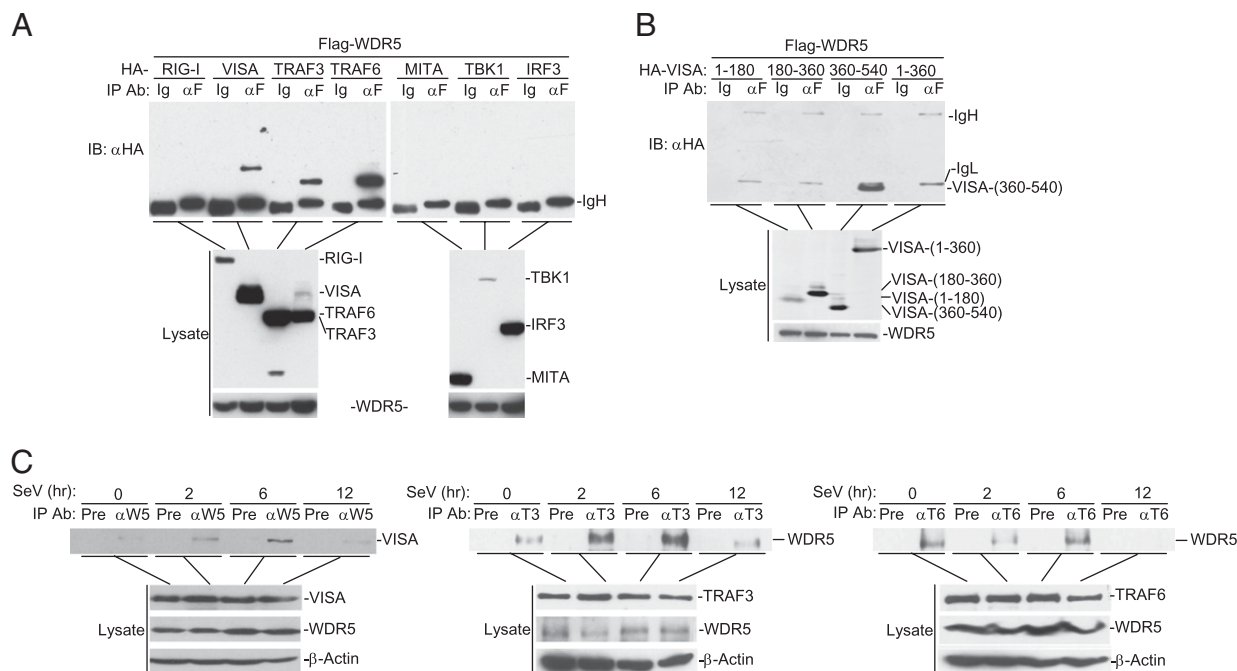


**Fig. 1.** WDR5 is associated with VISA, TRAF3, and TRAF6. (A) WDR5 interacts with VISA, TRAF3, and TRAF6 but not RIG-I, MITA, TBK1, or IRF3 in over-expression system; 293 cells ( $2 \times 10^6$ ) were transfected with the indicated plasmids (5  $\mu$ g each). Coimmunoprecipitation and immunoblot analysis were performed with the indicated antibodies (Upper). Expression of the transfected proteins were analyzed by immunoblots with anti-HA or anti-Flag (Lower). (B) Domain mapping of the VISA-WDR5 interaction. 293 cells ( $2 \times 10^6$ ) were transfected with the indicated plasmids (5  $\mu$ g each). Coimmunoprecipitation was performed with anti-Flag or control IgG. The immunoprecipitates were analyzed by immunoblot with anti-HA (Top). Expression of the transfected proteins were analyzed by immunoblots with anti-HA (Middle) or anti-Flag (Bottom). (C) WDR5 interacts with VISA, TRAF3, and TRAF6 in untransfected cells; 293 cells ( $5 \times 10^7$ ) were infected with SeV for the indicated time or left uninfected. Cell lysates were immunoprecipitated with the indicated antisera or control serum. The immunoprecipitates were analyzed by immunoblots with anti-VISA or anti-WDR5 as indicated (Upper). The levels of the proteins were analyzed by immunoblots with the indicated antibodies (Lower). Ig, control mouse IgG;  $\alpha$ F, anti-Flag; Pre, preimmune serum;  $\alpha$ T3, anti-TRAF3;  $\alpha$ T6, anti-TRAF6.

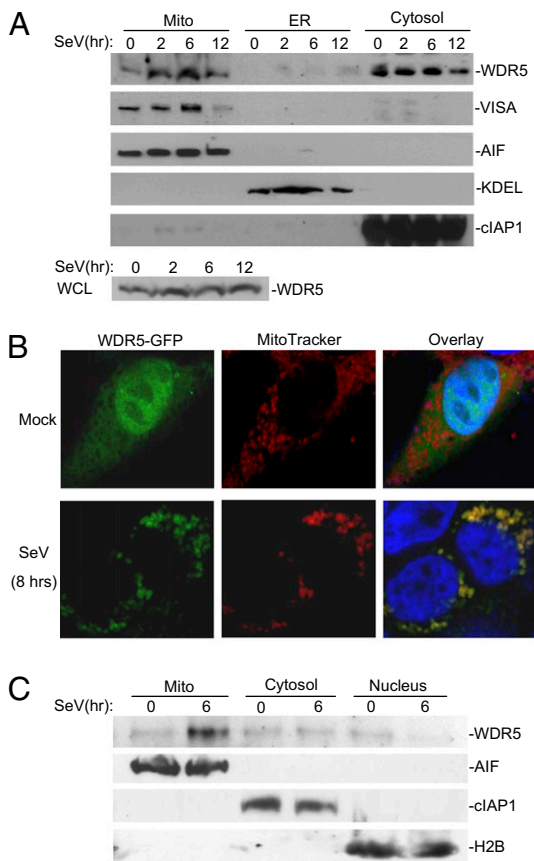


**Fig. 2.** WDR5 is translocated to the mitochondria after viral infection. (A) Cell fractionation and immunoblot analysis of the subcellular fractions; 293 cells were infected with SeV for the indicated time or left uninfected. Cell fractionations were performed; the fractions were equilibrated to equal volumes and analyzed by immunoblots with the indicated antibodies (Upper). The whole cellular levels of WDR5 upon viral infection were analyzed by immunoblot with anti-WDR5 (Lower). (B) Confocal microscopy of the cellular localization of WDR5; 293 cells were transfected with C-terminal GFP-tagged WDR5. Transfected cells were infected with SeV for 8 h or left uninfected before they were stained with the MitoTracker Red and observed under a confocal microscope. (C) Immunoblot analysis of the cellular localization of WDR5; 293 cells were infected with SeV for 6 h or left uninfected. The cells were fractionated and the subcellular fractions, including mitochondria, cytosolic fraction (cytoplasm without mitochondria and membranes) and nucleus, were equilibrated to equal volumes and analyzed by immunoblots with the indicated antibodies. WCL, whole cell lysate; Mito, mitochondria.

SeV infection (Fig. S3). As shown in Fig. 3B, the #3 RNAi construct could significantly inhibit SeV-induced activation of the IFN- $\beta$  promoter in reporter assays ( $P < 0.01$ ). Consistent with their effects on WDR5 expression, the #1 and #4 RNAi constructs had minor effects whereas the #2 RNAi construct had no inhibitory effects on SeV-induced activation of the IFN- $\beta$  promoter (Fig. 3B). Furthermore, knockdown of WDR5 also inhibited transcription of endogenous *IFNB1* gene (Fig. 3C). These results suggest that WDR5 is required for virus-triggered IFN- $\beta$  induction.

Activation of the IFN- $\beta$  promoter requires cooperative actions of IRF3 and NF- $\kappa$ B. Consistently, knockdown of WDR5 by the #3 RNAi construct significantly inhibited SeV-induced ISRE activation in reporter assays ( $P < 0.01$ ) (Fig. 3D) and IRF3 phosphorylation (Fig. 3E), which are hallmarks of IRF3 activation. Knockdown of WDR5 also inhibited SeV- but not IL1-induced NF- $\kappa$ B activation (Fig. 3F and G). These results suggest that WDR5 is specifically involved in SeV-induced IRF3 and NF- $\kappa$ B activation pathways.

To determine the molecular order of WDR5 in the virus-triggered signaling pathways, we examined the effects of WDR5 knockdown on ISRE activation mediated by components of the virus-triggered pathways. The results indicated that knockdown of WDR5 inhibited RIG-I-, RIG-I-CARD-, VISA-, and MITA- but not TBK1-mediated ISRE activation (Fig. 3H), suggesting that WDR5 acts downstream of RIG-I, VISA, and MITA but upstream of TBK1.

**WDR5 Is Essential for Assembly of the VISA-Associated Complex at the Mitochondria.** To further explore the mechanisms on the involvement of WDR5 in virus-triggered signaling, we determined the roles of WDR5 on the assembly of VISA-associated complex following viral infection. To do this, 293 cells were transfected with the #3 WDR5-RNAi plasmid and then infected or left uninfected with SeV for 6 h. The mitochondria were isolated and VISA-associated complex at the mitochondria was immunoprecipitated with anti-VISA antibody. Immunoblot analysis indicated that RIG-I was recruited to VISA in a viral infection dependent manner, whereas MITA, TRAF3 and TRAF6 were constitutively associated with VISA. Interestingly, knockdown of WDR5 expression by RNAi impaired virus-triggered association of VISA with RIG-I or MITA, as well as the constitutive association between VISA and TRAF3 or TRAF6 (Fig. 4). The impairment of assembly of VISA-associated complex was correlated with down-regulation of RIG-I and MITA at the mitochondria after WDR5 knockdown (Fig. 4). Because whole cellular levels of RIG-I and MITA were unchanged after WDR5 knockdown (Fig. S3), these results suggest that WDR5 is important for recruiting RIG-I and MITA to the VISA-associated complex on the mitochondrial membrane. Interestingly, the levels of TRAF3 and TRAF6 were not markedly changed after WDR5 knockdown, suggesting that WDR5 is not involved in recruiting TRAF3 and TRAF6 to the mitochondria but instead is important for the interactions between VISA and TRAF3 or TRAF6.

## Discussion

In most cell types, infection by RNA viruses is sensed by the cytoplasmic RNA helicase proteins RIG-I and MDA5. Recognition of viral RNAs by these helicase proteins results in induction of type I IFNs and other antiviral genes (10, 11). Elucidation of the molecular events of RIG-I and MDA5-mediated induction of type I IFNs is critical for understanding the complicated mechanisms of cellular antiviral innate immune response. Previous studies have revealed that the mitochondrial outer membrane protein VISA plays a central role in assembling a complex mediating virus-triggered IRF3 and NF- $\kappa$ B activation (13–16). However, the components of VISA-associated complex and their roles in virus-triggered signaling have not been fully defined. In this report, we identified WDR5 as a VISA-associated component required for virus-triggered activation of IRF3 and NF- $\kappa$ B as well as induction of IFN- $\beta$ .

Previously, it has been shown that WDR5 is a component of the MLL complex, which methylates lysine 4 of histone H3 (26–28). EST profile analysis indicated that WDR5 was ubiquitously expressed in most tissues. Cell fractionation experiments indicated that WDR5 was more abundantly localized in the cytoplasm than in the nucleus. These observations point to a previously unrevealed cytoplasmic function of WDR5. Using a TAP purification approach, we found that WDR5 was associated with VISA. Transient transfection and coimmunoprecipitation experiments indicated that VISA interacted with WDR5 constitutively. However, in untransfected cells, endogenous WDR5 was associated with VISA in a viral infection-dependent manner. These can be explained by two possibilities. Firstly, overexpression of VISA mimics its activation state as suggested by its ability to activate the IFN- $\beta$  promoter following its overexpression. Second, overexpression may detect weak interaction. In fact, many if not most

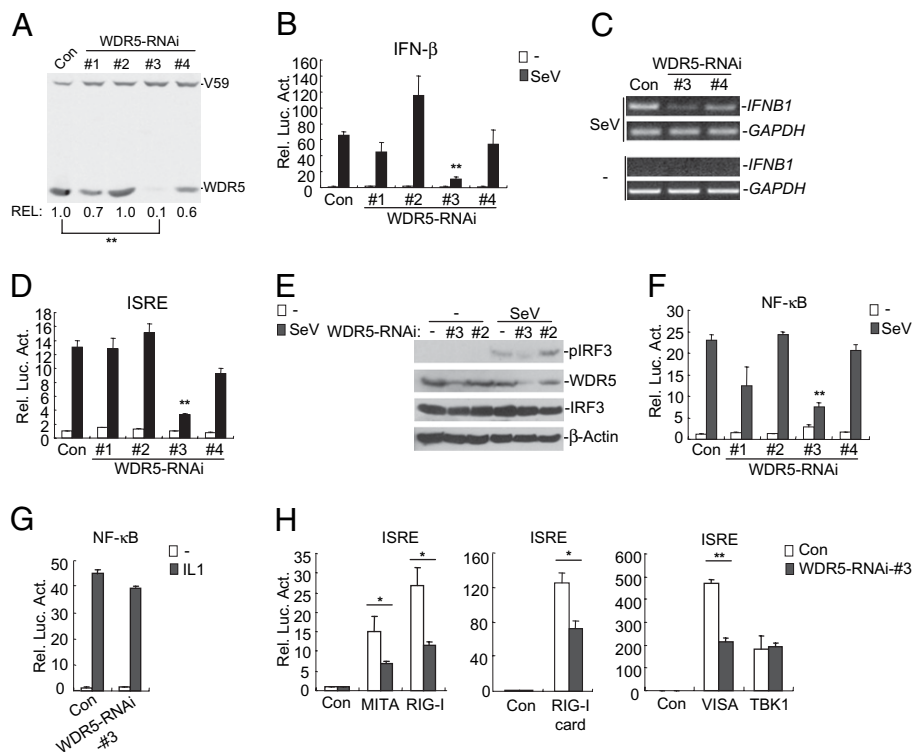


**Fig. 3.** Knockdown of WDR5 inhibits SeV-induced activation of IRF3, NF- $\kappa$ B and the IFN- $\beta$  promoter. (A) Effects of WDR5-RNAi plasmids on the expression of WDR5. 293 cells ( $2 \times 10^5$ ) were transfected with expression plasmids for Flag-WDR5 and Flag-V59 (0.1  $\mu$ g each), and the control or indicated WDR5 RNAi plasmids (1  $\mu$ g). Twenty-four hours after transfection, cell lysates were analyzed by immunoblot with anti-Flag. The WDR5 bands from three independent experiments were quantitated using the Bio-Rad Quantity One Program and normalized by levels of the control protein V-59. The average levels of WDR5 from the three experiments are shown at the bottom of the blot. \*\*,  $P < 0.01$ ,  $n = 3$ . (B, D, and F) Effects of WDR5-RNAi plasmids on SeV-induced activation of the IFN- $\beta$  promoter (B), ISRE (D), and NF- $\kappa$ B (F); 293 cells ( $2 \times 10^5$ ) were transfected with the indicated RNAi plasmids together with the indicated reporter plasmids. Cells were left uninfected or infected with SeV for 8 h before luciferase assays were performed. Graphs show mean  $\pm$  SD,  $n = 3$ . \*\*,  $P < 0.01$ . (C) Effects of WDR5 knockdown on transcription of endogenous *IFNB1* gene. 293 cells ( $2 \times 10^5$ ) were transfected with a control or the indicated WDR5-RNAi plasmids. Twenty-four hours after transfection, cells were infected with SeV for 6 h or left uninfected before RT-PCRs were performed with the indicated primers. (E) Knockdown of WDR5 inhibits SeV-induced IRF3 phosphorylation; 293 cells ( $2 \times 10^5$ ) were transfected with a control or the indicated WDR5-RNAi plasmids. Twelve hours after transfection, cells were selected with puromycin (1  $\mu$ g/mL) for 24 h, then infected with SeV for 6 h or left uninfected. Cell lysates were analyzed by immunoblots with the indicated antibodies. (G) WDR5-RNAi does not inhibit IL-1-induced NF- $\kappa$ B activation. 293 cells ( $2 \times 10^5$ ) were transfected with NF- $\kappa$ B reporter plasmid together with a control or WDR5-RNAi plasmid. Twenty-four hours after transfection, cells were left untreated or treated with IL-1 (20 ng/mL) for 8 h before luciferase assays were performed. Graphs show mean  $\pm$  SD,  $n = 3$ . (H) Knockdown of WDR5 inhibits RIG-I-, RIG-I-CARD, VISA-, MITA- but not TBK1-mediated ISRE activation. 293 cells ( $2 \times 10^5$ ) were firstly transfected with a WDR5-RNAi or control plasmid (1  $\mu$ g). Twenty-four hours later, cells were selected with puromycin (1  $\mu$ g/mL) for 24 h and then retransfected with ISRE reporter and the indicated expression plasmids (0.1  $\mu$ g each). Luciferase assays were performed 24 h after the second transfection. Graphs show mean  $\pm$  SD,  $n = 3$ . \*,  $P < 0.05$ ; \*\*,  $P < 0.01$ .

protein-protein interactions in various signal transduction pathways occur constitutively in overexpression system whereas in untransfected cells the interactions are stimulation-dependent.

Consistent with the observation that the interaction between VISA and WDR5 was viral infection dependent, viral infection caused translocation of WDR5 to the mitochondria, as revealed by both cellular fractionation and confocal microscopy experiments. Interestingly, viral infection caused down-regulation of WDR5 in the nucleus, suggesting that the mitochondrion-associated WDR5 may originate from the nucleus.

To investigate the roles of WDR5 in virus-triggered signaling, we determined the effects of WDR5 knockdown on virus-triggered IRF3 and NF- $\kappa$ B activation as well as induction of IFN- $\beta$ . Our results indicated that knockdown of WDR5 inhibited SeV-induced activation of IRF3, NF- $\kappa$ B as well as IFN- $\beta$  promoter, suggesting that WDR5 is required for virus-induced type I IFN signaling. Consistent with its association with VISA, knockdown of WDR5 inhibited upstream components RIG-I-, VISA-, and MITA- but not downstream component TBK1-mediated signaling. Because knockdown of WDR5 does not inhibit expression levels of RIG-I and MITA, these results together suggest

that WDR5 acts downstream of RIG-I and MITA and upstream of TBK1.

Previous studies suggest that overexpression of some of the signaling components of the virus-triggered pathways can activate IRF3, NF- $\kappa$ B, or both. However, overexpression of WDR5 failed to activate either IRF3 or NF- $\kappa$ B in reporter assays. This observation is not totally unexpected in light of the observations on other molecules in the pathways. For example, it is well established that IKK $\gamma$  is required for activation of NF- $\kappa$ B, whereas TRAF3 is required for virus-triggered IRF3 activation. However, overexpression of either IKK $\gamma$  or TRAF3 does not activate NF- $\kappa$ B or IRF3 (23, 24, 31).

In our experiments, we found that knockdown of WDR5 impaired the formation of the VISA-associated complex, providing an explanation of the critical role of WDR5 in virus-triggered type I IFN signaling. Knockdown of WDR5 caused down-regulation of RIG-I and MITA levels in the mitochondria after viral infection, whereas the whole cellular levels of RIG-I and MITA were unchanged after WDR5 knockdown. The simplest explanation for these observations is that WDR5 is important for recruiting RIG-I and MITA to the VISA-associated complex on the mitochondrial membrane. Knockdown of WDR5 also impaired the association of

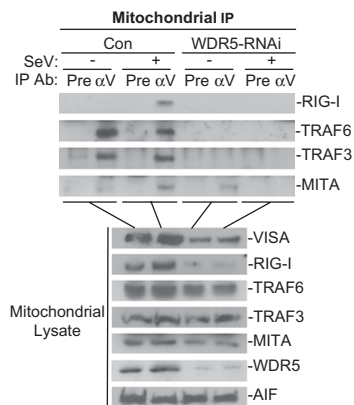


**Fig. 4.** Effects of WDR5 knockdown on assembly of the VISA-associated complex on the mitochondria. 293 cells ( $1 \times 10^8$ ) were transfected with a control or WDR5-RNAi plasmid. Twenty-four hours after transfection, cells were selected with puromycin ( $1 \mu\text{g}/\text{mL}$ ) for 24 h and then infected with SeV for 6 h or left uninfected. After infection, the mitochondria were collected by cell fractionation and the mitochondrial lysates were subjected to immunoprecipitation and immunoblot analysis with the indicated antibodies (*Upper*). Mitochondrial lysates were analyzed by immunoblots with the indicated antibodies (*Lower*). Pre, preimmune serum;  $\alpha\text{V}$ , anti-VISA.

VISA with TRAF3 or TRAF6 at the mitochondria. However, the levels of TRAF3 and TRAF6 in the mitochondria were not markedly changed after WDR5 knockdown. These results suggest that WDR5 is not involved in recruiting TRAF3 and TRAF6 to the mitochondria; instead, it is important for the interactions between VISA and TRAF3 or TRAF6. In conclusion, the identification of WDR5 as a component essential for assembly of VISA-associated complex after viral infection provides insights to the molecular mechanisms of virus-triggered type I IFN signaling and cellular antiviral response.

## Methods

**Reagents.** IL-1 (R&D Systems); MitoTracker Red (Molecular Probes); mouse monoclonal antibodies against Flag, HA and  $\beta$ -actin (Sigma), cIAP1 (R&D), AIF, KDEL, and H2B (Santa Cruz Biotechnology); rabbit polyclonal antibodies against TRAF3, TRAF6, and IRF3 (Santa Cruz Biotechnology), and phospho-IRF3 (Ser396) (Upstate) were purchased from the indicated manufacturers. SeV, rabbit anti-VISA, and mouse anti-RIG-I were previously described (16, 32, 33). Mouse anti-WDR5 antisera were raised against recombinant human WDR5.

**Constructs.** NF- $\kappa\text{B}$ , ISRE, and the IFN- $\beta$  promoter luciferase reporter plasmids, mammalian expression plasmids for HA- or Flag-tagged VISA and its mutants, RIG-I, TBK1, TRADD, FADD, RIP IRF3, TRAF3, TRAF6, and MITA were previously described (16, 18, 32, 33). Mammalian expression plasmids for HA-, Flag-, or GFP-tagged human WDR5 were constructed by standard molecular biology techniques.

**Protein Purification and Mass Spectrometry Analysis.** We firstly made a pCTAP-VISA construct, in which VISA cDNA was inframe fused to the C-terminal CBP and SBP tags in the pCTAP-A plasmid (Stratagene); 293 cells ( $5 \times 10^8$ ) stably transfected with pCTAP-VISA were collected and the cell lysate was subjected to tandem affinity purification procedures with the Interplay Mammalian TAP System (Stratagene). The purified VISA-associated proteins were digested by trypsin in solution. The tryptic peptides were analyzed by HPLC-ESI/MS/MS with a Thermo Finnigan LTQ adapted for nanospray ionization. The tandem spectra were searched against *Homo sapiens* National Center for Biotechnology Information reference database using the SEQUEST. Results was filtered by Xcorr  $+1 > 1.9$ ,  $+2 > 2.2$ ,  $+3 > 3.5$ , sp  $> 500$ , Deltcn  $> 0.1$ , Rsp  $\leq 5$ .

**RNAi.** Double-strand oligonucleotides corresponding to the target sequences were cloned into the pSuper.retro RNAi plasmid (Oligoengine). The target sequences for human WDR5 cDNA were as follows: #1: 5'-GCTGGGAA-TATCCGATGTA-3'; #2: 5'-GCGTGAGGATATGGGATG-3'; #3: 5'-GAATGAGAAATACTGCATA-3'; #4: 5'-CAGAGGATAACCTTGTTTA-3'.

**Transfection and Reporter Gene Assays.** 293 cells (approximately  $1 \times 10^5$ ) were seeded on 24-well plates and transfected the following day by standard calcium phosphate precipitation. To normalize for transfection efficiency,  $0.01 \mu\text{g}$  of pRL-TK or pRL-SV40 *Renilla* luciferase reporter plasmid was added to each transfection. Luciferase assays were performed using a dual-specific luciferase assay kit (Promega). Firefly luciferase activities were normalized based on *Renilla* luciferase activities. All reporter assays were repeated at least three times. Data shown were average values  $\pm$  SD from one representative experiment.

**RT-PCR.** Total RNA was isolated from 293 cells using TRIzol reagent (Invitrogen) and subjected to RT-PCR analysis to measure the expression of *IFNB1* and *GAPDH*. Gene-specific primer sequences were as follows.

*IFNB1*: 5'-CAGCAATTTTCAGTGTGTCAGCAAGCT-3' and 5'-TCATCCTGTCCTTGAGGCAGTAT-3';  
*GAPDH*: 5-AAAATCAAGTGGGGCGATGCT-3' and 5'-GGGCAGAGATGATGACCTTT-3'.

**Coimmunoprecipitation and Immunoblot Analysis.** For transient transfection and coimmunoprecipitation experiments, 293 cells (approximately  $1 \times 10^6$ ) were transfected for 24 h. The transfected cells were lysed in 1 mL of lysis buffer (20 mM Tris pH 7.5, 150 mM NaCl, 1% Triton, 1 mM EDTA,  $10 \mu\text{g}/\text{mL}$  aprotinin,  $10 \mu\text{g}/\text{mL}$  leupeptin, 1 mM phenylmethylsulfonyl fluoride). For each immunoprecipitation, 0.4 mL aliquot of lysate was incubated with  $0.5 \mu\text{g}$  of the indicated antibody or control IgG and  $30 \mu\text{L}$  of a 1:1 slurry of Protein G Sepharose (GE Healthcare) for 2 h. The Sepharose beads were washed three times with 1 mL of lysis buffer containing 500 mM NaCl. The precipitates were analyzed by standard immunoblot procedures.

For endogenous coimmunoprecipitation experiments, 293 cells ( $5 \times 10^7$ ) were infected with SeV for the indicated times or left uninfected. The coimmunoprecipitation and immunoblot experiments were performed as described above.

**Subcellular Fractionation.** Isolation of mitochondrial, membrane, and cytosolic fraction: 293 cells ( $5 \times 10^7$ ) infected with SeV or left uninfected were washed with PBS and lysed by douncing 40 times in 2 mL homogenization buffer (ApplyGen). The homogenate was centrifuged at  $500 \times g$  for 10 min. The supernatant (S5) was centrifuged at  $5,000 \times g$  for 10 min to precipitate mitochondria (P5K). The supernatant from this step (S5K) was further centrifuged at  $50,000 \times g$  for 30 min to yield the P50K, which contains the membrane fraction and the S50K, which mainly consists of cytosol.

Isolation of nuclear fraction: 293 cells ( $5 \times 10^7$ ) infected with SeV or left uninfected were washed with PBS and lysed by douncing for 40 times in 1 mL CER buffer (ApplyGen). The homogenate was centrifuged at  $500 \times g$  for 5 min and the pellet was saved as the crude nuclei, which was then washed twice with  $500 \mu\text{L}$  NER buffer (ApplyGen).

**Immunofluorescent Confocal Microscopy.** The 293transfected cells were left uninfected or infected with SeV for the indicated time. Cells were incubated with the MitoTracker Red (Molecular Probes) 30 min before the harvest. The cells were then fixed with 4% paraformaldehyde for 10 min and observed with a Leica confocal microscope under a  $\times 100$  oil objective.

**ACKNOWLEDGMENTS.** We thank Dr. Fuquan Yang and Mr. Peng Xue from the Institute of Biophysics at Chinese Academy of Sciences for their help with mass spectrometry. This work was supported by grants from the Chinese 973 Program (2006CB504301, 2010CB911802), the National Natural Science Foundation of China (30630019, 30700431, and 30921001), the Chinese Science and Technology Key Project (2008ZX10002-014) and the Chinese 863 program (2006AA02A306).

- Hiscott J (2007) Triggering the innate antiviral response through IRF-3 activation. *J Biol Chem* 282:15325–15329.
- Ishii KJ, Koyama S, Nakagawa A, Coban C, Akira S (2008) Host innate immune receptors and beyond: making sense of microbial infections. *Cell Host Microbe* 3:352–363.
- Yoneyama M, Fujita T (2008) Structural mechanism of RNA recognition by the RIG-I-like receptors. *Immunity* 29:178–181.

- Seth RB, Sun L, Chen ZJ (2006) Antiviral innate immunity pathways. *Cell Res* 16:141–147.
- Akira S, Uematsu S, Takeuchi O (2006) Pathogen recognition and innate immunity. *Cell* 124:783–801.
- Hiscott J (2007) Convergence of the NF- $\kappa\text{B}$  and IRF pathways in the regulation of the innate antiviral response. *Cytokine Growth Factor Rev* 18:483–490.

